Closed-Loop Control of Surface Preparation for Metallizing Fiber-Reinforced Polymer Composites

Shiva Shokri

A Thesis
in
The Department
of
Mechanical, Industrial
and
Aerospace Engineering

Presented in Partial Fulfillment of the Requirements
for the Degree of Master of Applied Science (Mechanical Engineering) at
Concordia University
Montreal, Quebec, Canada

November 2023

CONCORDIA UNIVERSITY

School of Graduate Studies

This is to certify that the thesis is prepared

By: Shiva Shokri

Entitled: Closed-Loop Control of Surface Preparation for Metallizing Fiber-Reinforced Polymer Composites

and submitted in partial fulfillment of the requirements for the degree of

Master of Applied Science (Mechanical Engineering)

complies with the regulations of the University and meets the accepted standards with respect to originality and quality.

Signed by the final Examining Committee:

_____ Chair

Dr. Martin D. Pugh

_____ Examiner

Dr. Martin D. Pugh

_____ Examiner

Dr. Farjad Shadmehri

_____ Supervisor

Dr. Tsz Ho Kwok and Dr. Mehdi Hojjati

Approved by _____

Dr. Martin D. Pugh, Chair of Department or Graduate Program Director

_____ _____

Date *Dr. Mourad Debbabi, Dean of Faculty*

Abstract

Closed-Loop Control of Surface Preparation for Metallizing Fiber-Reinforced Polymer Composites

by Shiva Shokri

To improve the surface properties of fiber-reinforced polymer composites, one method is to employ thermal spray to apply a coating on the composite. For this purpose, it uses a metal mesh serving as an anchor between the composite and the coating to increase adhesion. However, the metal mesh is covered by resin, and getting an acceptable coating is only possible through an optimum exposure of the metal mesh by sand blasting prior to coating. Therefore, this study aims to develop a closed-loop control system to inspect and blast the parts properly. Specifically, this approach takes the top-view images from a microscope as the inputs. A convolutional neural network (CNN) is trained to correlate these images with the corresponding exposure levels of the metal mesh, measured by a destructive method. Then, this trained CNN model can estimate the exposure level by only analyzing the top-view images. Finally, it serves as a feedback mechanism to guide the subsequent sandblasting operations. The state-of-the-art has only examined the sand-blasted composites manually, requiring expertise and experience. This method automates the inspection process efficiently with an inexpensive portable digital microscope. The experimental results show that the method can distinguish the status of surface preparation successfully, and it is practical in closed-loop control. This study also has applications to various fields of manufacturing for defect detection and closed-loop control.

Acknowledgements

I wish to express my deepest gratitude to my esteemed supervisor, Prof. Tsz Ho Kwok and my co-supervisor, Prof. Mehdi Hojjati, whose unwavering guidance, support, and invaluable encouragement have played an indispensable role in my journey through the M.A.Sc program. Without a doubt, this project would have been impossible to undertake without their expert supervision, profound insights, and dedicated mentorship. I extend my heartfelt appreciation and thanks to my friends, and dedicated research colleagues, including Shima Akhondi, Christopher Danny-Matte, Eder da Silva Sales, Maksudul Alam, and Ankhy Sultana, for their kind support and assistance. I would also like to express my deep appreciation to the committee members, Dr. Martin Pugh and Dr. Farjad Shadmehri, for their valuable contributions to this endeavor.

Contents

List of Figures

List of Abbreviations

FRPC	Fiber Reinforced Polymer Composite
LPPS	Low-Pressure Plasma Spray
VPS	Vacuum Plasma Spray
CS	Cold Spraying
TWAS	Twin-Wire Arc Spraying
APS	Air-Plasma Spraying
HVOF	High-velocity Oxygen Fuel
SPS	Suspension Plasma Spray
SPPS	Solution Precursors
TBC	Thermal Barrier Coating
MAE	mean absolute error
MSE	mean-squared error
PSNR	peak signal-to-noise ratio
SSIM	Structural Similarity Index Measure
CV	Computer Vision
IoU	Intersection Over Union
ML	Machine Learning
DL	Deep Learning
ANN	Artificial Neural Networks
CNN	Convolutional Neural Network
CNN-R	Convolutional Neural Networks with Regression
FC	Fully Connected
AFP	Automated Fiber Placement

RTM	Resin Transfer Molding
AM	Additive Manufacturing
SOD	Stand-Off Distance

1 Introduction

Fiber reinforced polymer composites (FRPCs) are getting more popular in a broad range of applications, such as aircraft and spacecraft, watercraft, wind turbine, offshore platform, automobile, recreational equipment, and chemical container [1]. FRPCs are attractive because of their significant specific strength, superior longevity, and corrosion resistance. In addition, it is possible to manufacture complex geometries with fewer parts using FRPCs and thus reduce the manufacturing cost [2]. However, FRPCs have some limitations including lack of high-temperature resistance, deficient impact strength, and relatively low thermal and electrical conductivity. These have caused in-service failures, e.g., erosion of wind turbine blades [3], ice accumulation and lightening strike on airplanes [4], impairment in aircraft caused by bashing of other flying objects such as birds, and fire damages to navy ships. To enhance the performance of FRPCs, the state-of-the-art technology [5] has implemented surface modification by deposition of metallic coating on the composites employing thermal sprays. Thermal spray coatings on fiber-reinforced polymer composites are often used to enhance their mechanical, thermal, or protective properties. One real-life example can be found in the aerospace industry, where thermal spray coatings are applied to fiber-reinforced polymer composites used in aircraft components. For instance, aircraft engine components, such as turbine blades or combustion chamber liners, are often subjected to extreme temperatures and harsh environments. To improve their resistance to wear, corrosion, and thermal degradation, thermal spray coatings can be applied to the surface of fiber-reinforced polymer composite components. In the thermal spray coated turbine blades, the coating acts as a thermal barrier, protecting the underlying polymer composite from the high temperatures generated during engine operation. Moreover, the coating provides resistance

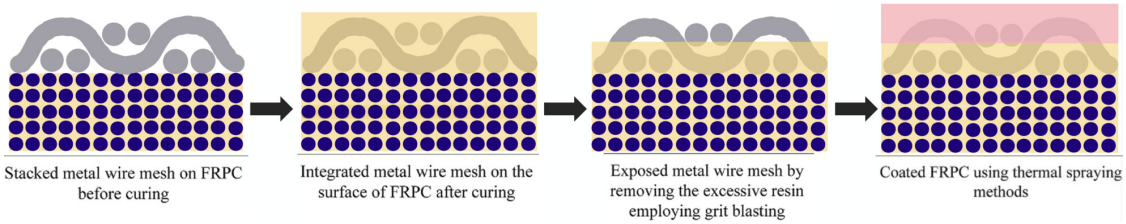

FIGURE 1.1: Illustration of preparing FRPC for surface metalization via the incorporation of metal wire mesh on the surface of the composite.

against wear and corrosive elements present in the engine environment. The combination of fiber-reinforced polymer composites and thermal spray coatings enhances the overall durability and performance of the turbine blades. In general, these coatings can contribute to extending the service life of critical engine components [3]. Nevertheless, applying metallic surface coatings on FRPCs using thermal spraying methods is a disputable process, primarily because of the sensitivity of the composite to high temperature, as well as its low impact-strength [6].

Recent research [7] has substantiated the efficacy of a novel strategy for addressing the limitations of FRPCs through the integration of a metal wire mesh onto the composite surface prior to the curing phase (see Fig. 1.1). This innovative technique establishes a robust foundation for the subsequent deposition of metallic coatings, facilitating this process without compromising composite integrity. During the curing stage, the resin infiltrates the interstices of the metal mesh, fostering comprehensive integration within the composite matrix. Subsequent to the curing process, the resin encapsulates the metal mesh, necessitating a meticulous grit blasting procedure to eliminate superfluous resin and achieve an optimal level of metal mesh exposure. This deliberate abrasion augments surface roughness, thereby rendering it conducive for the subsequent deposition of metallic particles, while simultaneously enhancing coating adhesion strength through mechanical interlocking mechanisms. Grit blasting, although potent, harbors inherent aggressiveness that potentially jeopardizes the structural integrity of FRPCs. Accordingly, prior works have meticulously explored parameter optimization to mitigate potential damage. However, the inherent variability associated with both the test samples and the grit blasting procedure introduces the possibility of over-blasted or

under-blasted outcomes. Consequently, a comprehensive inspection of the grit-blasted surface and its exposure level emerges as a prerequisite prior to embarking upon the subsequent costly thermal spraying process. The challenge is further compounded by the fact that the thickness of the excessive resin layer typically measures in the order of 100 microns, rendering it barely discernible to the naked eye. The current methodology for inspecting grit-blasted FRPCs primarily involves extracting a small sample from the component, followed by a microscopic analysis. Regrettably, this approach is both destructive and manual in nature, making it impractical for widespread industrial application. Furthermore, its accuracy is susceptible to fluctuations due to operator expertise, fatigue, and other variables.

These imperatives serve as the driving force behind our research initiative aimed at designing an in-situ closed-loop control system tailored to govern the grit blasting process. The practicality of this system hinges on its ability to embody traits of affordability, speed, robustness, and nondestructiveness. However, the requirement for nondestructiveness implies that conventional cross-sectional analysis through sample cutting is precluded, leaving us with the option to exclusively examine the samples from a top-down perspective. During our preliminary investigation, it was observed that the extent of exposure distinctly influences the surface texture attributes as observed through a portable microscope. Consequently, we posit a hypothesis suggesting a discernible linkage between the patterns manifested on the surface and the corresponding level of metal mesh exposure. Establishing such a correlation would permit the acquisition of surface images solely from a top-view stance of the FRPC surface while retaining the capability to govern the resin height within acceptable parameters during grit blasting. The successful realization of this proposed system holds the potential to not only address the aforementioned challenges but also to revolutionize surface preparation methodology by introducing a more methodical and intricate approach.

To examine this hypothesis, we adopt a methodical experimental approach. Initially, we create a series of FRPC samples, varying their exposure levels systematically through controlled grit blasting. Subsequently, utilizing a cost-effective and portable

digital microscope, we capture images of the upper surface of each sample. In the analytical phase, we harness a convolutional neural network (CNN) to scrutinize the images and unveil potential meaningful connections between surface patterns and exposure degrees. By training the CNN, it can comprehend texture attributes and establish correlations with the documented exposure levels of the metal mesh across individual samples. To delve deeper, we integrate the CNN with regression analysis (referred to as CNN-R), allowing us to numerically gauge the intensity and characteristics of the relationship. Successful validation of the hypothesis hinges on identifying a distinct and statistically substantial correlation between surface patterns and exposure levels. Should this validation materialize, the hypothesis could serve as a foundational component for a closed-loop control mechanism during the grit blasting process. In this context, the CNN-R fusion serves as an instrumental monitoring instrument. It estimates the exposure level and conveys this data into a feedback control system. Within this system, the measured exposure percentage is juxtaposed against a desired exposure threshold (a set point). Consequent adjustments to the control parameter – specifically, the grit blasting pressure – are iteratively executed until an optimal exposure level is reached, striking a balance that avoids excessive treatment while achieving the desired outcome. The study's contributions are summarized as follows:

1. A meticulously crafted control system is introduced, leveraging an affordable and portable digital microscope to capture top-surface images of FRPC samples. These images are pivotal for the quantification of surface patterns and texture attributes.

2. The research employs a robust image analysis approach, utilizing convolutional neural networks with regression (CNN-R), to establish a statistically significant correlation between surface patterns and exposure levels of the underlying metal mesh.

3. The incorporation of the CNN-R model for exposure level estimation contributes to a closed-loop control system for grit blasting pressure. This innovative system offers a streamlined and effective avenue for achieving meticulous surface preparation.

The experimental results show that the correlation achieves an impressive accuracy rate of 95%. The proposed system significantly curtails material wastage, ensures uniform quality, and provides a practical solution for attaining precise outcomes. The thesis is organized as follows: Chapter 2 first reviews the related works. Then, Chapter 3 presents the proposed method and the algorithms developed for analyzing the acquired data. After that, Chapter 4 shows the results, and finally, Chapter 5 concludes the thesis.

2 Literature Review

This work is related to composite coating, vision-based inspection, and closed-loop control. They are reviewed in this section.

2.1 Composite coatings

The manufacturing of FRPCs has garnered significant attention due to their versatility in various applications [8]. Nevertheless, challenges persist regarding their in-service performance [6, 4]. Many of these challenges are related to surface phenomena, which can be addressed through surface engineering and functionalization [9]. It is worth noting that the process of enhancing the properties of FRPCs through surface coatings holds great promise for broadening the spectrum of applications for these composites and simultaneously curbing waste and maintenance expenses. This, in turn, contributes to the overarching goal of sustainable development. A significant facet of FRPCs that has received relatively less attention from the scientific and industrial communities pertains to surface engineering and the application of coatings on this class of materials. In the following section, we provide a concise overview of the prominent coating method which has been utilized in this work, shedding light on its types, respective strengths and limitations when it comes to depositing protective and functional films onto FRPC substrates. This discussion aims to offer insights into the potential and challenges associated with surface engineering in the context of FRPCs.

2.1.1 Thermal spraying methods

Thermal spraying is a well-established industrial technique employed for surfacing and resurfacing engineered components. This method offers a versatile approach to deposit

a wide range of materials, including metals, alloys, metal oxides, metal/ceramic blends, carbides, wires, rods, and various composite materials, onto diverse substrate materials. This results in the creation of unique coating microstructures or near-net-shape components. Thermal spraying techniques use heat sources and for these processes, gases, and in certain instances, air, are employed to facilitate the introduction of materials into the gun and to generate the requisite heat for the melting process. The high velocities of these gases lead to the material being expelled as fine molten droplets, which subsequently impact the target part, undergo solidification, and adhere to its surface. The bonding mechanism is primarily mechanical, although there are cases where metallurgical bonding also occurs. This results in each layer forming a robust connection with the preceding layer, giving rise to a lamellar structure reminiscent of a "pancake-like" splat. The properties of the resultant coating are intricately linked to the interplay between kinetic and thermal energy during the process. The primary objective of thermal spray coatings is to furnish a functional surface that can either safeguard or modify the behavior of a substrate material or component. This technology finds extensive application across a multitude of industries worldwide. Its diverse range of functions includes restoration and repair, corrosion protection, resistance against various forms of wear like abrasion, erosion, and scuff, as well as heat insulation or conduction. Thermal spray coatings are also applied in scenarios involving oxidation and hot corrosion, electrical conductivity or insulation, near-net-shape manufacturing, seals, engineered emissivity, abradable coatings, decorative purposes, and more. There are five fundamental thermal spray processes, each with its unique characteristics:

1. Flame spray powder/wire, detonation, and High Velocity Oxygen Fuel (HVOF) processes are combustion-based methods. Among these, HVOF and detonation spraying are recognized for their high bond strength and exceptionally dense microstructures [10].

2. Plasma and wire arc processes employ electric energy to aid in melting consumable materials. Plasma coatings, when applied using Low-Pressure Plasma Spray

(LPPS) or Vacuum Plasma Spray (VPS) Systems, exhibit high bond strength and relatively dense, oxide-free microstructures.

Additionally, there is a relatively new process known as Cold Spray, which relies more on high velocity and kinetic energy than thermal energy. In Cold Spray, particle temperatures are lower than in HVOF, but velocities are significantly higher. This approach results in coating structures that closely resemble bulk wrought materials [5]. Beyond the material being deposited, the primary differentiating factor among these studies is the method employed to enhance adhesion strength without compromising the substrate.

Flame Spray

Flame spraying, considered the earliest thermal spray method, employs the high temperature generated by gas combustion flames, which can reach approximately 3000 °C (depending on the gas-oxygen ratio), as the heat source for melting powder or wire feedstock. While this method is cost-effective, it presents certain limitations, including relatively low coating adhesion, high porosity, and oxide content. Moreover, the involvement of an open flame in the process restricts its application for Fiber-Reinforced Polymer Composites (FRPCs), which can be flammable. The challenges with flame spraying in the context of FRPCs are further compounded by the need to maintain a minimal standoff distance between the spraying gun and the substrate (typically in the range of 150-250 mm) to mitigate oxide content in the coating. This, in turn, reduces the risk of compromising the integrity of the polymeric base substrate. However, research has shown that applying a garnet sand/epoxy layer to the FRPC substrate before flame spraying can limit heat transfer and hinder the degradation of the composite during the flame spraying process, especially when applying materials like Al-Si and NiCrAlY on FRPCs [11, 12].

High Velocity Oxygen Fuel (HVOF)

Continuous ignition within a combustion chamber, where a mixture of liquid or gaseous fuel combined with oxygen or ambient air is present, results in the generation of a high-velocity stream of hot gas. This gas forms the basis for thermal spraying and is expelled through a nozzle. HVOF (High-Velocity Oxygen Fuel) and HVAF (High-Velocity Air Fuel) systems provide extreme temperatures reaching up to 3000 °C and accelerate the feedstock particles to speeds ranging from 600-1200 m/s, depending on the type of fuel and oxidant gas composition. These methods are known for depositing coatings with remarkable density and superior adhesion when compared to plasma-sprayed coatings. However, the high kinetic energy of semi-molten particles sprayed using HVOF and HVAF may pose a risk to the surfaces of polymeric and FRPC substrates. Still, they hold potential for applying coatings to surface-modified substrates through techniques such as using a bond coat and/or metallic mesh. Recent research highlights successful efforts to deposit Al-Si coatings on FRPCs by employing intermittent HVOF spraying in combination with cooling the substrate using compressed air [10].

Twin-Wire Arc Spray

The twin wire arc spray gun operates by utilizing direct electrical current to create an electric arc between two conductive consumable wires, reaching extremely high temperatures ranging from 4000 to 6000 °C. This intense heat source melts the wire feedstock, while compressed air or noble gases (used to minimize oxidation) atomize the molten wire feedstock, propelling particles at velocities between 50 and 150 m/s toward the substrate. This method stands out due to its high spraying rate and low power consumption, making it remarkably cost-effective. Furthermore, its ability to handle various materials in the form of cored wire feedstock extends its applicability [13]. Controlling several key parameters is crucial when applying wire arc spraying to coat low melting point substrates. These parameters include current, atmosphere, feeding rate, substrate temperature, standoff distance, and surface treatment of the substrate. Notably, surface preparation through laser texturing on the substrate has proven effective

in enhancing coating adhesion. This enhancement results from the mechanical anchoring of particles on the textured surface [14]. Additionally, the deposition of a pure zinc bond coat, which exhibits suitable wettability on non-metallic substrates, shows promise for creating build-up coatings on Polymer Matrix Composites (PMCs) [15]. In the context of thermoplastics, studies on employing wire arc spraying for coatings reveal challenges when depositing metals with low density and/or high melting points onto thermoplastics with high impact strength. This challenge arises because the particles either lack the required momentum to adhere to the surface or they cause localized melting without proper deposition [13].

Plasma Spray

Plasma spraying is a potent technique that relies on a DC-generated electric arc, bridging the gap between a copper anode and tungsten cathode, to ionize the primary plasma gas (typically Ar or He). Once the gas reaches an energy level conducive to recombining free electrons and gas ions, it forms a high-energy plasma jet. This plasma jet generates a substantial amount of energy and light, elevating temperatures to levels as high as 15,000 °C. This intense heat serves a dual purpose: it acts as the heat source for melting the feedstock and imparts a drag force to propel the molten particles toward the substrate. Although plasma spraying is widely used in industry, it encounters challenges related to torch arc instabilities and electrode wear, particularly with tungsten electrodes [16]. To address these issues, it has been reported that, in addition to secondary plasma gases such as H2 and N2, modulating the current can be employed instead of varying the power input. This modulation helps better control arc fluctuations, subsequently influencing the properties of the plasma jet and the resulting coatings [17]. When it comes to feedstock, plasma spraying supports the use of various materials, including dry powders, wires, suspensions (SPS), and solution precursors (SPPS). The limitations associated with spraying nano and ultrafine dry powders have led to the development of SPS and SPPS. One of the key advantages of plasma spray, aside from its low oxide content, is its versatility in depositing coatings ranging from highly dense to porous

while maintaining acceptable adhesion by adjusting spraying parameters. Beyond its conventional use in depositing coatings, particularly thermal barrier coatings (TBCs) on metallic substrates [18], recent research highlights the feasibility of metallizing polymers and low melting point substrates using plasma spray methods [19]. In fact, the inclusion of a powder filler layer, such as Cu powder [20], Al bond coat [14], or metal wire mesh [21], before plasma spraying has proven effective for successfully depositing coatings on FRPCs.

Cold Spray

Cold spray is a process that involves the utilization of heated, highly compressed gas. This gas is directed into a converging-diverging nozzle, enabling it to reach supersonic velocities. The high-speed gas serves to accelerate solid particles, propelling them with significant kinetic energy. These particles, upon impact with the substrate, either deform plastically or penetrate it. As a result, optimizing key parameters, such as gas pressure, temperature, particle size, and spraying distance, is crucial for achieving a successful coating. Despite the fact that the sprayed particles are in solid form and relatively cool, their kinetic energy is substantial enough to erode polymeric and FRPC substrates, similar to HVOF and HVAF processes. However, it's worth noting that successful deposition of low-melting-point powders on thermoplastic substrates has been reported, underscoring the potential use of cold spray for metallizing FRPCs. Several studies have explored the deposition of tin (Sn) coatings on FRPCs using cold spray, with findings indicating higher deposition efficiency at lower temperatures and pressures (below 500 K and 60 psi). However, it's important to be cautious, as increasing certain cold spray parameters can lead to erosion of the composite and fracture of fibers [22, 23, 24, 25].

2.1.2 Thermal spraying benefits and challenges

The attractiveness of thermal spray processes lies in their user-friendliness, cost-effectiveness, and their advantageous attributes that cater to a wide array of industrial applications.

The advantages typically encompass reduced costs, improved engineering performance, and/or extended component lifespan. This makes thermal spray a valuable and versatile technique, widely embraced by industries across the globe. Various thermal spraying methods have not only evolved to facilitate the deposition of a diverse array of materials but also to control specific factors such as particle temperature, velocity, and size. The manipulation of these parameters enables the creation of coatings that fulfill specific requirements, including considerations like porosity, adhesion, and functionality [17]. However, the coating or metallization process for FRPCs still presents uncertainties. For instance, due to the properties of FRPCs, during contact with thermal spray particles, the composite may experience erosion or deformation through partial melting and re-solidification [22]. In this context, thermoplastic matrices have shown greater suitability for direct surface metallization compared to thermosetting ones [23]. Nonetheless, the high viscosity of thermoplastic resin leads to manufacturing defects that hinder proper fiber coverage [26]. Conversely, thermosetting composites, owing to their low viscosity and resin flow, ensure thorough wetting of fibers, significantly reducing defects [27]. Nevertheless, various thermal spraying methods, including dynamic cold spraying (CS), flame spraying, twin-wire arc spraying (TWAS), air-plasma spraying (APS), and high-velocity oxygen fuel (HVOF), have successfully achieved surface metallization of FRPCs [10]. Notably, approaches such as electroplating or thermally spraying a thin metallic bond coat [28], applying a blend of garnet grit/epoxy [12], spraying a mixture of metal/thermoplastic powder [29], and more recently, incorporating a metal wire mesh on the uppermost surface of the FRPC [7], have been systematically explored. The latter approach, in particular, can provide a versatile anchor for the coating with robust adhesive strength, albeit contingent on the exposure level of the metal mesh. It is important to note that achieving this exposure is accomplished through grit-blasting, which must be carefully executed and inspected to ensure a uniform texture of roughened metal mesh.

2.2 Computer Vision-based Inspection Techniques

Up to date, all the inspections during grit-blasting for surface preparation have been done manually by just taking a look at the grit-blasted surface through a microscope. Followed by that, the decision making has always been affected by human eye errors and long duration of manual analysis. In fact, vision is human's most sophisticated and advanced sense. This explains why images play the most important role in a human's perception. Imaging machines, in contrast to human, are not limited to the visual band of the electromagnetic (EM) spectrum and can cover almost the entire EM spectrum, ranging from gamma to radio waves [30]. Even though computer and human vision are functionally similar, you cannot expect a computer vision system to exactly copy the function of the human eye. Computer vision techniques have the capacity to replicate and even enhance human vision systems [31]. These techniques find widespread application in tasks such as classification [32], industrial automation, quality control, and defect detection [33, 34], among others. In the preceding sections, we have delved into some of the most prominent and widely adopted computer vision techniques in the industry.

2.2.1 Feature Detection

Visual feature detection, encompassing elements like points, edges, and lines, serves as the foundation for many computer vision (CV) algorithms. In certain scenarios, the focus is on specific regions within an image, such as human eyes, license plates, or corner shapes, which we refer to as keypoint features. Conversely, other situations emphasize identifying the edge features of objects present in an image. Some CV algorithms are designed to detect and match both keypoint and edge features across different images. The assessment of feature detection quality typically relies on several widely used evaluation metrics. These metrics include the mean absolute error (MAE), mean-squared error (MSE), peak signal-to-noise ratio (PSNR), and the structural similarity index measure (SSIM). They provide a quantitative means of evaluating the accuracy and performance

of feature detection algorithms, ensuring they meet the desired quality and precision standards.

Keypoint detection

Keypoint detection methods can be broadly categorized into two primary types: local search detection and global search detection. Within local search detection, there are various techniques like correlation methods, least squares methods, and learning-based methods [35]. Local search detection methods are particularly well-suited for scenarios where images are captured continuously and at a high frequency, such as in video sequences. In contrast, global search detection methods take a different approach. These methods involve searching the entire image comprehensively and then matching features based on their appearance. As a result, global search methods are more apt for situations characterized by substantial movement or changes in the appearance of the scene [36]. This approach is effective in scenarios where you need to consider a broader context or the entire image to identify relevant keypoints.

Edge detection

Edges within images frequently occur at the boundaries separating different objects, manifesting as abrupt changes in color and intensity. One established technique for detecting edges relies on assessing the image's gradient [37], although this gradient measurement can be sensitive to noise. Consequently, a low-pass filter, such as a Gaussian filter, is commonly employed to preprocess the image before calculating the gradient. Edge recognition can involve horizontal and vertical convolution operations. Another technique involves the zero-crossing method, where the zero points of a second-order derivative expression are identified to pinpoint edges [38]. Notably, deep-learning methods, especially convolutional neural networks (CNNs), have gained significant traction in the realm of edge detection [39]. These modern approaches leverage the power of CNNs to enhance the accuracy and robustness of edge detection algorithms,

allowing for more reliable results, even in the presence of complex and noisy image data.

2.2.2 Recognition

Recognition is a pivotal task in computer vision (CV) techniques. When we consider target objects, recognition problems can be categorized into three primary groups:

1. Instance Recognition
2. Class Recognition
3. General Category Recognition
4. Action Recognition

In assessing the performance of recognition algorithms, several common evaluation metrics come into play, including accuracy, recall, precision, F1 Score, and ROC/AUC curves. These metrics provide a quantitative means to measure the effectiveness of recognition models [40].

Instance recognition

In the realm of instance recognition, the primary objective is to pinpoint and identify a particular known object. Various strategies are employed to tackle this recognition challenge:

1. Feature Matching: This involves comparing the distinctive features of the target object with those in the scene to identify a match. Feature matching strategies are commonly employed in this context [36].
2. Viewpoint-Invariant Feature-Based Strategies: These methods are designed to recognize objects regardless of changes in their viewpoint. They focus on identifying consistent features that remain even when the object is viewed from different angles [41].

3. Sparse Feature Matching: In this approach, recognition relies on identifying and matching only the most salient and discriminative features within an image or scene, which is particularly useful for efficient instance recognition [42].

An illustrative application of instance recognition is found in the domain of face recognition [43], where the aim is to identify specific individuals. These various techniques and methods contribute to the diverse toolkit available for solving instance recognition challenges, spanning from feature matching to advanced machine learning approaches.

Class recognition

In contrast to instance recognition, class recognition differs in that it doesn't target specific individual objects. In class recognition, the objective is typically to identify whether an image contains an instance of a specific object category, like cars or pedestrians. Class recognition can be viewed as a specialized classification problem, where the input is an image, and the output is the classification of that image. In the evolutionary timeline of computer vision (CV), the proliferation of Convolutional Neural Networks (CNNs) stands out as a pivotal advancement that has driven the recent rapid progress in CV technologies. Over recent years, a multitude of CNN architectures have emerged and found applications in classification tasks, with models progressively growing in complexity [40].

General category recognition

General category recognition represents the most intricate challenge in the realm of recognition, as it necessitates not only pinpointing the positions of diverse objects in an image but also ascertaining the specific category to which each object belongs. This task demands the recognition of a wide array of objects present in the image. In addressing the complexities of general category recognition, several approaches have been employed, including bag-of-words models and part-based models. Bag-of-words models involve comparing the distribution of visual words within the target image to the patterns identified during training [44]. In part-based models, the image is dissected

into distinct parts, each examined separately to determine the presence and location of objects of interest. Recent progress in this field has harnessed the power of deep residual learning and deep neural networks [45] to enhance the performance of general category recognition systems.

Action recognition

Another challenge in the field of recognition is action recognition, a task that humans naturally excel at but poses significant difficulties for machines. The accurate identification of actions and behaviors in videos holds tremendous importance across various applications. For instance, it plays a vital role in scenarios like monitoring pedestrian movements in autonomous driving systems and detecting falls among the elderly. In the realm of the manufacturing industry, recognizing the behaviors of workers within a workshop setting has proven to be a valuable approach for ensuring production safety [46, 47].

2.2.3 Segmentation

Image segmentation, a fundamental task in the field of computer vision, is concerned with assigning pixels to distinct groups based on the objects they belong to. This process is akin to a clustering problem. Early segmentation methods often employed techniques involving region division and merging. Later approaches integrated indicators of consistency, including intraregional coherence and interregional dissimilarity. As an instance, in a previous work [2], we designed a region growing technique for segmenting and clustering the resin on FRPC surface images. Other segmentation techniques such as mean shift, graph-based merging, graph cut-based Markov methods, and level sets [48, 49, 50] have been developed. In learning-based segmentation algorithms, common loss functions include the Dice loss, rooted in the Dice coefficient, and the intersection over union (IoU) [51].

2.2.4 3D modeling

In the realm of computer vision, 3-D modeling is typically categorized into two distinct problems: stereo correspondence and 3-D reconstruction. Stereo correspondence pertains to the process of creating a 3-D model of an object by analyzing two or more images of the same object or scene. Conversely, 3-D reconstruction aims to generate a 3-D model of an object based solely on a single image [52]. Assessing the quality of a predicted 3-D point cloud in comparison to the ground truth poses a notable challenge, often requiring the design of an effective loss function. One approach involves evaluating how well the projections of the predicted 3-D point clouds align with the silhouette of the ground-truth object [53, 54].

2.3 Composite Surface Image Analysis

Image analysis plays a significant role in composite manufacturing and coating processes by providing insights into the quality, defects, and characteristics of materials [34]. Here are some examples illustrating the role of image analysis in this context:

1. Fiber Orientation Analysis: Image analysis can determine the alignment of reinforcing fibers in composite materials. By analyzing microscopic images of composite cross-sections, manufacturers can ensure that fibers are properly oriented, which is crucial for the material's strength and performance [55].

2. Porosity Detection: Image analysis can identify and quantify the presence of voids and pores in composite structures. High-resolution images can reveal even tiny defects that might weaken the material. This information is essential for quality control [56].

3. Bond Line Inspection: In composite bonding processes, image analysis can check the integrity of adhesive layers. It can identify any gaps or defects in the bond line between composite parts [57].

4. Coating Thickness Measurement: Image analysis can be used to measure the thickness of coatings applied to composite surfaces. By analyzing the color or intensity variations between the coating and the substrate, manufacturers can ensure coatings meet the specified thickness requirements [58, 59].

5. Defect Detection: Image analysis helps in identifying defects such as cracks, blisters, or delaminations in coatings. These defects can compromise the protective or decorative functions of the coating [60].

6. Surface Roughness Assessment: Image analysis can evaluate the surface roughness of coatings. Understanding the texture of the coating is essential in applications where smoothness or adhesion is critical [61].

7. Pattern Recognition: Image analysis can be used to recognize specific patterns or features on composite materials, such as identifying product labels or barcodes. This is particularly useful in tracking and tracing products throughout the manufacturing and distribution process [62].

8. Process Monitoring: Image analysis can monitor manufacturing processes in real time. For example, in thermal spray coating, cameras can capture images of the coating process, and image analysis software can detect anomalies or variations that may affect the coating quality [63].

In a primary research on automatic FRPC surface inspection [2], we developed an image analysis algorithm where the resin clusters distribution was compared by histograms for determining the state of grit blasting. As depicted in Fig. 2.1, the surface image is segmented into resin and metal regions and the resin-covered areas are mapped by pseudo colors. The histograms indicate that the resin clusters change in size and distribution as the grit blasting state changes from under-blasted to over-blasted and it can be fitted by a Gaussian curve. In a later research, we developed an image processing technique based on the experimental and manual results of [64] where the focus was on calculating the metal wire lengths as a feature to determine the surface exposure level to grit blasting. With respect to this approach, we fitted rectangles to metal mesh segments

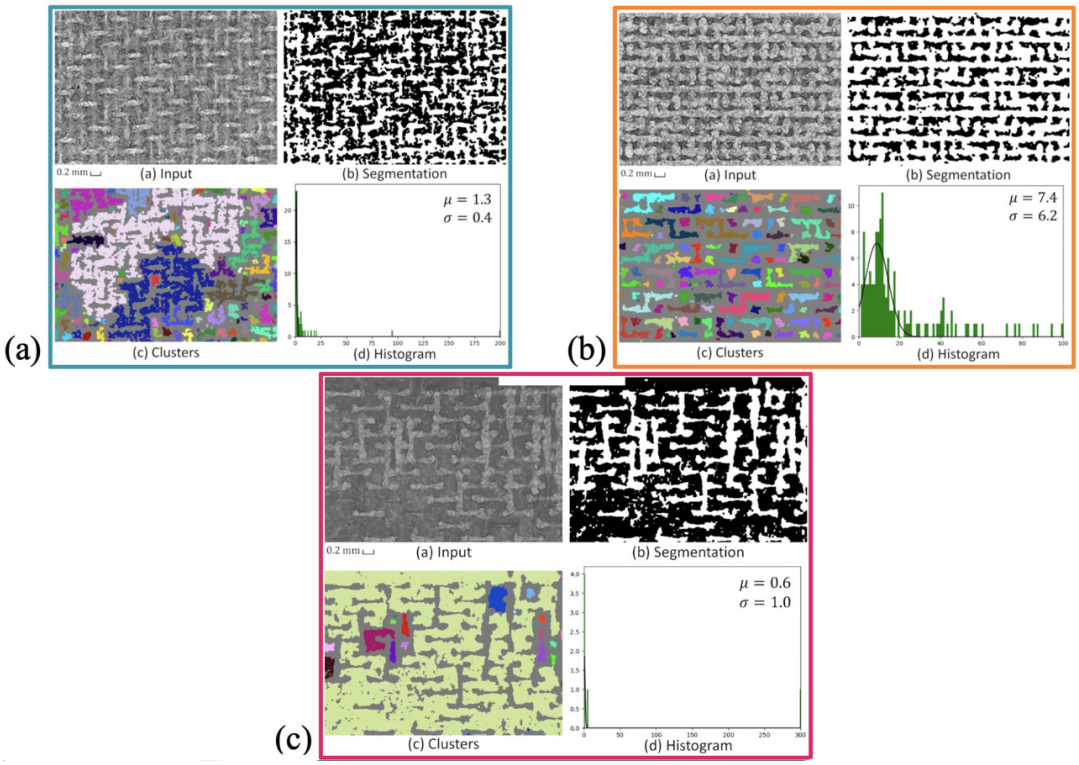

FIGURE 2.1: Statistical surface image analysis for three samples with histograms. (a) Under-blasted. (b) Properly blasted. (c) Over-blasted

on the top view images of FRPCs and analyzed the distribution of wire segment lengths in properly blasted and under-blasted samples by histograms. Fig. 2.2 is an overview of our second methodology based on computer vision contributing towards an automatic surface exposure calculation. In summary, image analysis is instrumental in ensuring the quality and consistency of composite manufacturing and coating processes. It helps detect defects, assess material properties, and monitor production, contributing to the overall performance and reliability of composite materials and coated surfaces.

2.3.1 Machine learning in composite surface image analysis

Much of the ongoing research in this field focuses on devising effective methods for extracting crucial information and features, such as distributions that accurately depict the inner content and attributes of images [65, 2]. Notably, texture is one of these critical features, playing a significant role in characterizing the quality of various products particularly in the realm of surface analysis for composites [66]. Despite the advancements

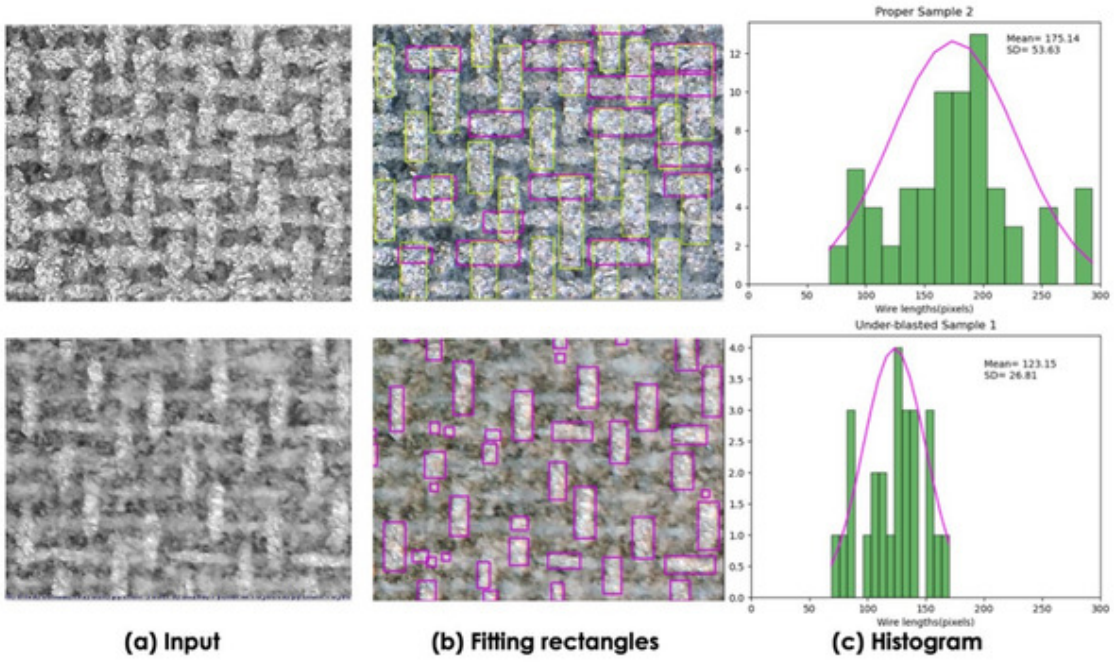

FIGURE 2.2: Histogram results for wire segment lengths calculated in two random properly blasted (up) and under-blasted (down) samples by our shape fitting method.

in surface texture analysis, the sensitivity and specificity of these methods remain sub-optimal [67]. Image texture analysis systems that utilize ML techniques are fast evolving in recent years. ML techniques include decision tree learning, clustering, support vector machines (SVMs), k-means nearest neighbor (KNN), restricted Boltzmann machines (RBMs) and random forests (RFs) [68]. Still, the pre-requisite for ML techniques to work efficiently is the extraction of discriminant features which are generally unknown, and the tasks of manual feature extraction are always sensitive and challenging. Among the most commonly utilized approaches is the deployment of Convolutional Neural Networks (CNNs), which belong to the class of artificial neural networks (ANNs) [69]. CNNs have made substantial contributions to various domains within image analysis due to their minimal need for preprocessing [70, 71, 72, 73]. These networks possess the remarkable ability to autonomously optimize their filters (kernels) through a process of automated learning [74].

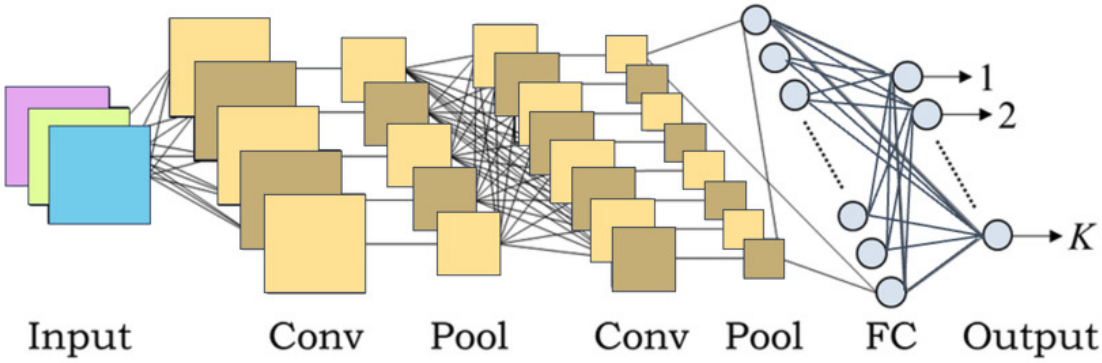

FIGURE 2.3: An example of CNN architecture

2.3.2 Convolutional Neural Networks

The Convolutional Neural Network (CNN) is a feedforward neural network designed to automatically extract features from data using convolutional structures. In contrast to conventional feature extraction methods [41], CNN eliminates the need for manual feature extraction. The CNN architecture draws inspiration from the human visual system [75], where artificial neurons correspond to biological neurons, CNN kernels act as receptors responsive to various features, and activation functions simulate the transmission of neural electric signals exceeding a certain threshold to the next neuron. A basic CNN architecture is depicted in 2.3. Additionally, loss functions and optimizers are introduced to train the CNN system to learn specific patterns. CNN offers several advantages when compared to fully connected (FC) networks. These include:

1. Local Connections: Neurons are no longer connected to all neurons in the previous layer but only to a limited set, effectively reducing parameters and expediting convergence.

2. Weight Sharing: Groups of connections can share the same weights, further reducing parameters.

3. Dimension Reduction through Downsampling: Utilizing pooling layers, CNN leverages the principle of local correlation in images to downsample, reducing data volume while retaining valuable information. This process can also eliminate trivial features.

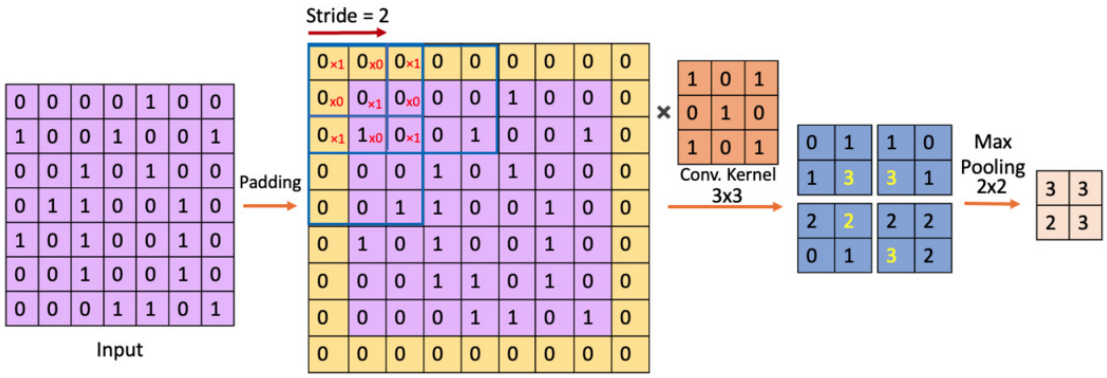

FIGURE 2.4: The general convolution and feature extraction procedure in a CNN

Convolution is a pivotal step in feature extraction, resulting in feature maps. However, convolution can lead to information loss at the borders. Padding, introducing additional zero values around the input, helps adjust sizes indirectly. Strides control the density of convolution. Larger strides reduce density [76, 77]. Following convolution, feature maps contain numerous features, which may lead to overfitting. To address this, pooling (also known as downsampling) methods, such as max pooling and average pooling, eliminate redundancy [78]. The entire CNN process is outlined in Fig. 2.4. In this example, the input image is convolved with a 3x3 kernel in the convolutional layer which is though of as the "eyes" of CNN. At each epoch, CNN updates its filters (kernels) to progressively learn the patterns by analyzing small chunks of data acquired as feature maps. In summary, CNNs are essential deep learning algorithms that automatically extract features from data, inspired by the principles of biological vision and characterized by local connections, weight sharing, and downsampling to enhance efficiency and reduce the risk of overfitting [79]. Consequently, a significant advantage of CNNs lies in their independence from prior knowledge and the need for human intervention in feature extraction. Therefore, CNNs are also employed in our work.

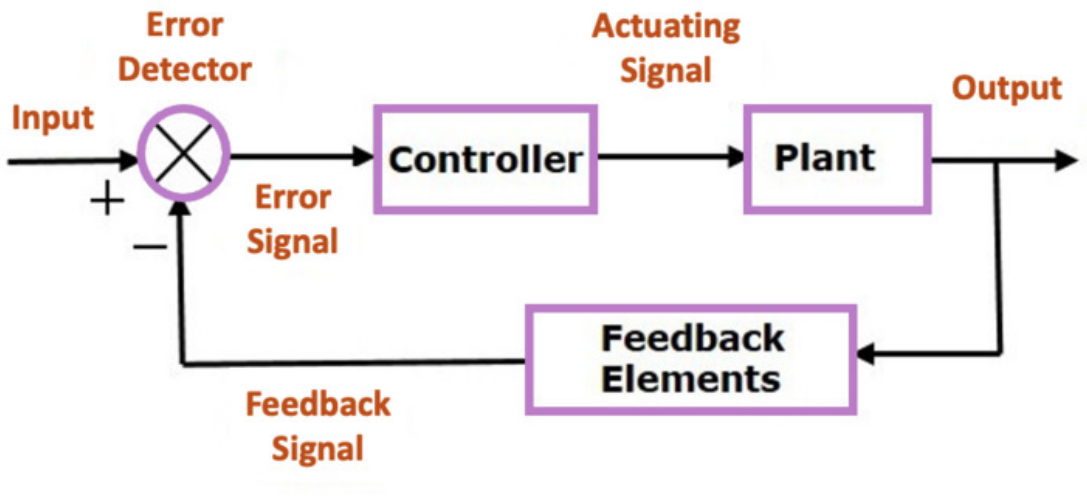

FIGURE 2.5: The block diagram of a simple feedback control system

2.4 Closed-loop control in composite manufacturing

In many systems, especially those involving control, there's often a specific variable that needs to be maintained at a desired value. Consider the example of an inverted pendulum control system, where the goal is to keep the pendulum in a vertical position by moving a cart horizontally. Closed-loop control systems, like this one, typically consist of three main components:

- Sensor: This component measures a key variable of interest, such as the angle of the pendulum concerning the vertical position.
- Actuator: It's the element that changes the system's state to adjust the controlled variable (e.g., an electric motor on the cart moves the cart to control the pendulum).
- Controller or Processor: Often seen as the "brain" of the system, it utilizes data from the sensor to compute the appropriate action to drive the actuator, thereby achieving the desired control action [80].

Figure 2.5 depicts the block diagram of a simple closed-loop control system. The control system's logic, or "controller," can be implemented on a computing device, whether it's

a standard computer or a smaller, resource-constrained device like a microcontroller. One crucial aspect of a closed-loop system is stability. System stability ensures that the state variables remain close to their desired set points over time. Instability can lead to problems like actuator saturation, oscillations, or, in the worst case, the system spiraling out of control [81, 82]. Closed-loop control in composite manufacturing refers to a systematic approach where real-time data is continuously collected from the manufacturing process, analyzed, and then used to make immediate adjustments to ensure that the final composite product meets the desired specifications. This approach provides a feedback mechanism that allows manufacturers to maintain consistent quality, improve efficiency, and reduce waste [83]. The utilization of data analytics and machine learning methods has emerged as a prominent trend in the pursuit of achieving optimal feedback control. Here are some examples to illustrate closed-loop control in composite manufacturing:

- Curing Process in Fiber-Reinforced Composites: In the manufacturing of fiber-reinforced composites, the curing process is critical. Closed-loop control can be applied to ensure that the temperature, pressure, and curing time are precisely controlled. Sensors continuously monitor temperature and pressure within the curing oven, and this data is sent to a controller. If the temperature deviates from the setpoint, the controller can adjust the heating elements accordingly to bring it back into the desired range. This results in the establishment of precise control over the curing environment, and the detection of flaws in composite materials [84].

- Composite Layup in Automated Fiber Placement (AFP): Automated Fiber Placement is a process where composite fibers are accurately placed on a mold or substrate to create complex shapes. Closed-loop control involves monitoring the position and tension of the fibers in real-time. If the system detects any deviation from the desired fiber placement, it can make immediate adjustments to correct it. For example, if the tension in a fiber becomes too high, the system can slow down the placement or adjust the tension to prevent breakage. As instance, in a study, a

hybrid system encompassing both position and force control was employed. This system communicates critical information to the industrial robot controller, allowing for precise tool corrections and enhancing overall process accuracy [85]. This approach demonstrated improved homogeneity, leading to enhanced mechanical performance.

- Material Mixing in Resin Transfer Molding (RTM): In the RTM process, resins and other additives are mixed to create the composite material. Closed-loop control can be used to monitor the viscosity and composition of the resin mixture. If the mixture deviates from the desired viscosity or composition, the system can adjust the flow rates of the individual components to maintain the correct mixture. This ensures that the composite material is consistent and meets the required specifications [86].

- Quality Inspection and Defect Detection: After the composite is manufactured, closed-loop control can also be applied to quality inspection. Automated inspection systems use various sensors, such as cameras and ultrasound, to detect defects or inconsistencies in the final product. If a defect is identified, the system can trigger an alarm and, in some cases, even make real-time adjustments to correct the issue. For instance, if a defect is detected during the automated trimming process, the trimming tool's path can be adjusted to remove the defect while preserving the good material [87, 88, 89]. In a recent study, a closed-loop framework was introduced, which integrates advanced deep learning models into robot-based composite additive manufacturing systems [90],. This framework facilitates the development of a closed-loop adjustment system that corrects process parameters upon detecting defects through deep learning.

Furthermore, the enhancement of various aspects of composite recycling has been explored through the use of artificial neural networks (ANNs) [91]. Researchers have also delved into the application of advanced control algorithms to manage the complexities of composite manufacturing [92]. Consequently, closed-loop control systems in composite manufacturing help to ensure that the final products meet the required quality

standards, reduce waste, and improve overall process efficiency. They play a crucial role in achieving consistent, high-quality composite materials used in various industries, from aerospace to automotive and beyond. Despite these recent advancements, research in this emerging field highlights a significant gap, emphasizing the absence of a comprehensive and cohesive strategy aimed at facilitating automatic adjustments and informed decision-making in the process of preparing FRPC surfaces for coating. Given the novelty of this method, there is a limited body of work addressing the monitoring and optimization aspects specific to this process.

3 Methodology

To fabricate the metal mesh/FRPC assembly, CYCOM® 977-2 prepregs (carbon fibers pre-impregnated with epoxy resin and partially cured) are combined with stainless steel 316 wires in a 200-mesh configuration. A unidirectional laminate comprising 20 layers of CFRP prepreg ($[0]_{20}$) is meticulously arranged on a prepared tool. Subsequently, a cleaned metal mesh is overlaid onto the laminate, and the entire setup is enclosed in a vacuum-sealed bag, ready for autoclave curing. Following fabrication, the top of the polymer composite hosts a layer of resin that obscures the metal mesh. The challenge is to selectively remove a portion of the resin, providing sufficient surface area on the metal mesh for subsequent coating. In Fig. 3.1, a microscope view displays a FRPC sample featuring the metal mesh covered by resin. The objective is to ascertain the resin's depth and determine whether the sample is primed for coating. Ideally, the resin thickness should be half the height of the metal mesh, ensuring that a significant portion of the mesh remains exposed to serve as an anchor for the coating on the composite surface. For analysis, a low-cost ($\sim$ \$100) USB microscope with 40× magnification and 1080×1920 resolution, commonly available in the market, is employed to capture images. These images are then subjected to machine learning techniques to ascertain the level of exposure, enabling quantification of the percentage of metal mesh surface exposed. The subsequent sections elaborate on the intricacies of this method.

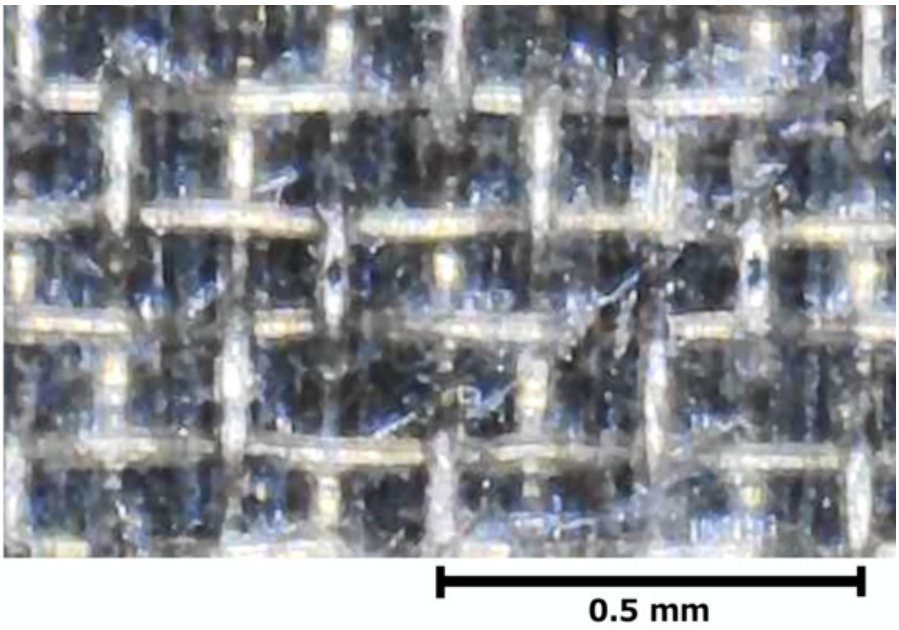

FIGURE 3.1: FRPC before grit blasting with metal mesh on its surface fully covered with resin

3.1 Experimental setup and data generation

3.1.1 Grit Blasting

The experimental configuration is illustrated in Fig. 3.2. To achieve uniform grit blasting across the surface, the procedure involves securing the sample onto a surface covered by a protective film. This film acts as a safeguard for fixture components, mitigating potential damage during the grit blasting process. For controlled and even motion, the sample is set in motion along both the X and Y directions through the utilization of a X-Y table. This setup is connected to an external controller situated outside the grit blasting cabinet, facilitating the activation and deactivation of the motors during grit blasting. Furthermore, to maintain a consistent position and angle, the grit blasting gun is affixed to a fixture. During each pass of the grit blasting process, the sample undergoes a prescribed sequence of movements. Initially, it experiences horizontal motion from left to right along the X axis. Subsequently, it transitions to vertical movement, progressing from the bottom to the top while moving along the X axis. This choreographed sequence of movements guarantees complete and thorough exposure of the sample's

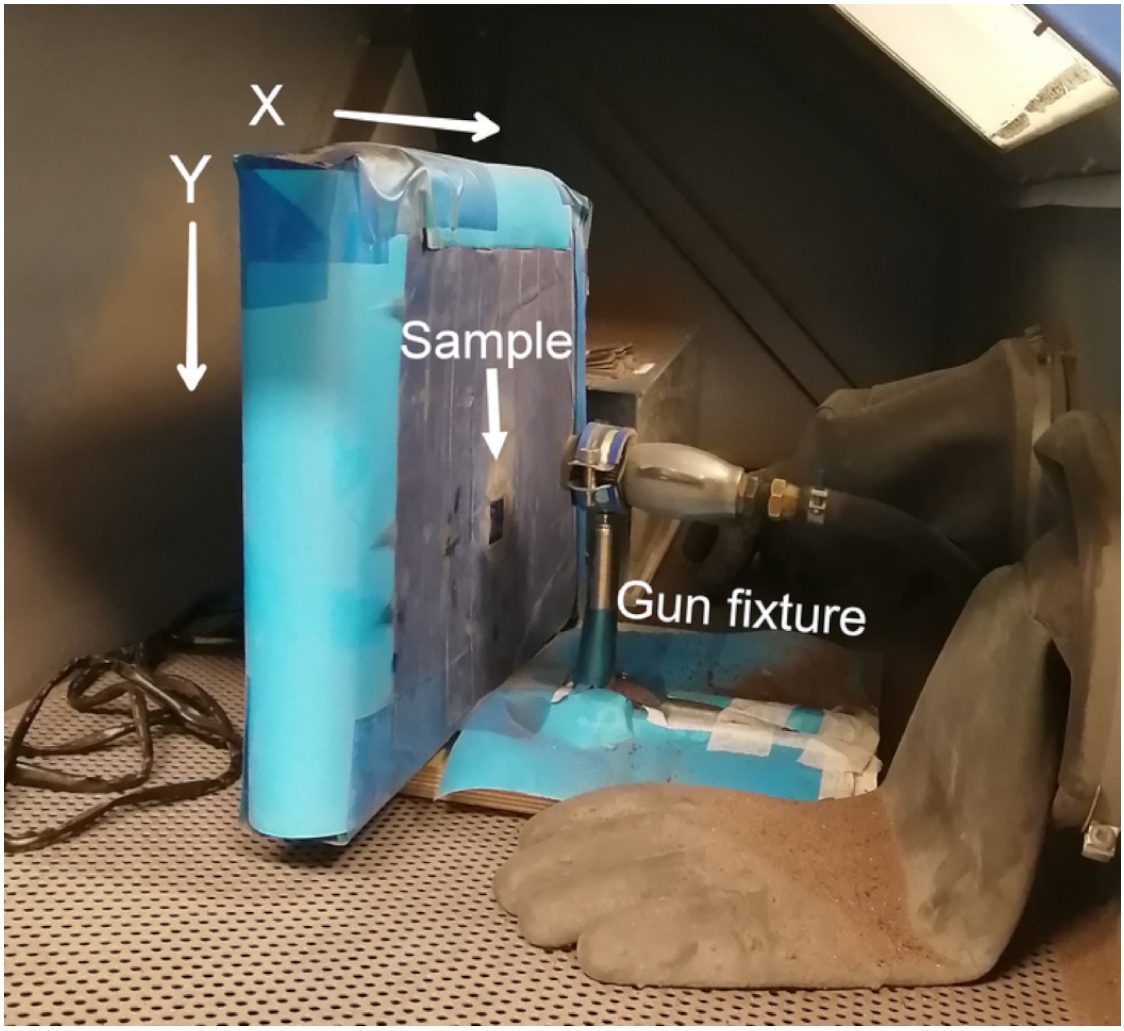

FIGURE 3.2: Experimental setup for data generation: the sample and gun fixtures are placed inside a cabinet covered with a protective film.

surface to the grit blasting process, ensuring a comprehensive treatment. The experimental design encompasses a comprehensive spectrum of grit blasting states, ranging from under-blasted to over-blasted conditions. This is accomplished by carefully adjusting three crucial parameters: air pressure, stand-off distance (SOD), and number of passes. All other factors, such as gun angle, particle size, grit material, and speed, are held constant with regards to the grit blasting procedure designed in [64]. Specifically, the air pressure levels are set at 60, 80, and 100 psi; SODs at 3, 4, and 5 inches; and the number of passes at 1, 2, and 3. Consequently, a total of 27 distinct grit-blasted samples are generated. The exposure levels of these samples are quantified using a destructive

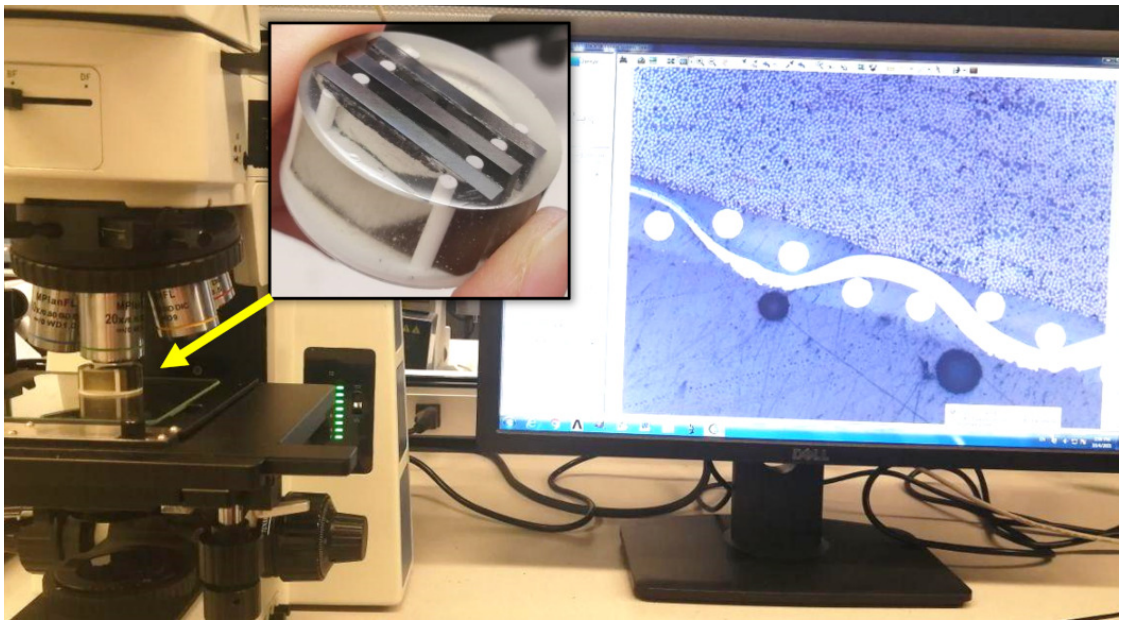

FIGURE 3.3: Mesh in resin side view. An image of the coupons prepared for grit-blasting, sample cut in half, and samples mounted for polishing and characterization by optical microscope.

approach involving an optical microscope (Fig. 3.3).

3.1.2 Ground Truth

Analyzing the cross-section of the initially produced samples and the surface of polished samples prompted the concept of establishing a correlation between the metal wire mesh exposure level and the length of exposed wires when viewed from the top [64]. Notably, a significant innovation in this study is the utilization of a compact, cost-effective, portable digital microscope for the assessment of composites from a top-view perspective, eliminating the need for destructive testing of the sample. The "Skybasic handheld digital microscope," featuring a magnification range of 50-1000, is employed. This microscope is equipped with 8 LEDs, allowing for adjustable light intensity, a valuable feature for achieving a clear contrast between metal and polymer due to their distinct light reflection properties. To achieve the correlation between the metal wire exposure level and the length of exposed wires when viewed from the top, the average height of exposed wires calculated from the cross-section view (h), was acquired as a

function of the average length of exposed wires from the top view (x) which was manually calculated by ImageJ software. This correlation was achieved through interpolation of coordinates of several points on the wire curve [64]. It's important to note that in an ideal scenario, where the metal wire mesh exhibits precise dimensions without any irregularities, the maximum value of x would correspond to an exposure level of 50%. As a result, referring to h(x), the exposure percentage for each top-view image is calculated and recorded as the ground truth.

3.1.3 Image Data Generation

In fact, each sample is subjected to image capture at five different locations, yielding a collection of 135 surface images. Without loss of generality, the samples are captured at a right angle, ensuring that the metal mesh wires are positioned vertically and horizontally in the images. Alternatively, automatic rotation can be implemented to align the wires correctly if they are not initially well-oriented. Images are subsequently resized by 50% to incorporate a more comprehensive mesh pattern within the receptive field. These images are further cropped into smaller 256×256 resolution images, yielding 450 images per initial capture. Furthermore, we augmented the image data by incorporating various conceivable variations into the data set. Given that all samples are initially positioned at right angles during capture, we apply rotations of 90, 180, and 270 degrees, as well as vertical and horizontal flips. This augmentation results in a total of 2,700 images for each captured image. These images are labeled according to their corresponding exposure level percentage (e.g., 29.9) which is the ground truth. In total, this leads to 36,900 labeled images across 17 exposure levels. The data set is divided into training and validation sets, with 32,400 images for training and 4,500 images for validation. The division ensures an even distribution of exposure levels across both sets, encompassing the entire spectrum from under-blasted to over-blasted samples.

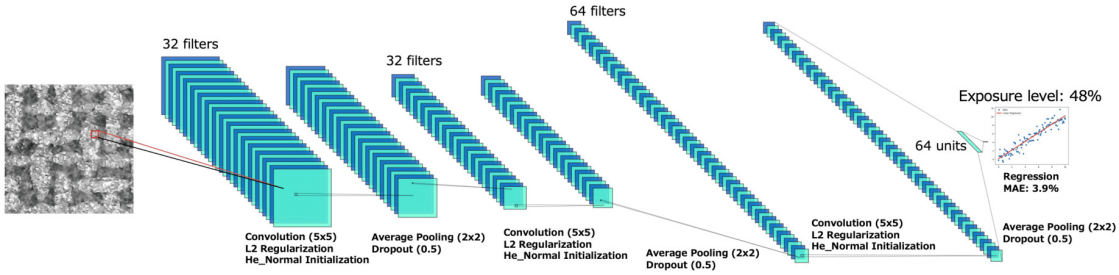

FIGURE 3.4: The proposed CNN Architecture

3.2 Convolutional Neural Network with Regression

Convolutional Neural Networks (CNNs) are a class of deep neural networks well-suited for processing visual imagery due to their incorporation of convolutional computation. They can be viewed as regularized versions of fully connected neural networks, as they exploit hierarchical patterns in data by assembling intricate structures from smaller, simpler patterns extracted using convolution filters [73]. Drawing on the proven success of CNNs, we employ them to extract texture features from surface images captured from the top view of grit-blasted FRPCs, aiding in estimating surface exposure levels. The CNN model is implemented using Keras with TensorFlow backend on a Python IDE. Keras preprocessing leverages the ImageDataGenerator class, generating tensor image data batches with real-time augmentation. This class facilitates labeling image data and creating training and testing sets for the CNN. The CNN architecture includes three convolutional layers (as depicted in Fig. 3.4) for texture feature extraction. Each layer performs dot-product multiplication of input vectors with trainable weights and biases to uncover internal features. The output of the first layer flows into the second, and then into the third for progressively higher-level feature extraction. Rectified linear unit (ReLu) activation functions and average-pooling layers follow each convolutional layer. Activation functions introduce non-linearity, while pooling layers down-sample input data to extract distinctive features along the spatial dimension. To mitigate over-fitting, a dropout layer randomly discards some of the first layer outputs. This prevents the network from failing when predicting new data. The outputs of the final convolutional

layer are flattened and fed into a fully connected layer. Given that the output is a continuous value estimating exposure percentage, a regression layer with a single unit and a linear activation function is appended at the end.

Specifically, the input surface images are fed into the convolutional layers using filters (kernels) of size $FW \times FH \times N$, where FW, FH, and N denote the filter width, height, and depth, respectively. The first convolutional layer, applied to the input image ($IW \times IH$), changes the output image shape to a size of

$$[\frac{IW - FW + 2p}{S} + 1, \frac{IH - FH + 2p}{S} + 1, N],$$

where IW and IH are the input width and height, while S and P represent the stride and padding values, respectively. The forward computation of the CNN structure is expressed as:

$$X_{i+1}^{l} = f_a(k_{i,i+1}^{l} x_i^{l-1} + b_{i+1}^{l}),$$

where X_{i+1}^{l} represents the output feature map i+1 in the l^{th} layer, $k_{i,i+1}^{l}$ signifies the kernel linking feature map i in the $(l-1)^{th}$ layer to the output feature map $i+1$ in the l^{th} layer, b_i is the bias matrix tied to the output feature map $i+1$ in the l^{th} layer, and f_a denotes the activation function, which is set as ReLU. ReLU is adopted due to its capability in enforcing non-saturation and nonlinearity in both positive and negative phase information of the CNN output [93]. The kernel of the CNN enhances the feature representation of input data. The output layer is directed to a cost function, yielding mean squared error (MSE):

$$y = \frac{\sum_{i=1}^{n} (x_i^l - o_i^l)^2}{n}.$$

In this equation, n represents the number of training data points, and o_i^l is the observed data. The entire learning process aims to minimize this loss function via the back-propagation algorithm, which computes derivatives of the loss throughout the network. The back-propagation phase employs the ADAM optimizer for training and minimizing the cost function. The average-pooling layer is independently applied to feature maps for down-sampling and enhanced feature extraction. This layer computes mean

values from a fixed region of the convolutional layer without multiple filter depths. This downsizes the data and enhances feature extraction. The fast convergence and improved feature generalization in the average-pooling layer are captured by

$$f_m(x^l) = Average(x_i^l),$$

where $f_m(x^l)$ denotes the average-pooling results of the l^{th} CNN layer. In this study, dropout is employed after the first convolutional layer and its subsequent activation function for effective regularization and prevention of over-fitting. The dropout layer randomly disregards output nodes from the previous layer. During training, the dropped nodes are temporarily excluded by %10 in the forward network, resulting in the corresponding weight and bias parameters remaining unaltered in the backward network. Consequently, the network becomes less sensitive to irrelevant weight and bias values, leading to improved generalization on unseen data and a reduced risk of overfitting [76].

Prior to commencing training, it's imperative to initialize weights and biases of the network to activate neurons for propagation. As the proposed CNN employs ReLU activation functions, the He Normal technique is chosen for weight initialization [94]. Moreover, regularization is crucial to counter over-fitting, where a model becomes adept at training data but fails with unseen test data. This is seen when training error drops, but validation error remains high. It signifies learning specifics rather than trends. Model complexity, tied to sensitivity to minor changes, leads to focusing on trivial details, causing misguided learning. By controlling complexity through regularization, influenced by model weights and feature count, sensitivity can be managed [95]. Integrating a regularization term minimizes complexity and loss simultaneously. In this context, L2 regularization is applied. It supplements the cost function with a penalty term composed of the squared magnitude of coefficients:

$$J(\theta) = \frac{1}{m}\sum_{i=1}^{m} Cost(h_\theta(x^i), y^i) + \frac{\lambda}{2m}\sum_{j=1}^{n} {\theta_j}^2,$$

where m represents data size, n denotes the number of features, and λ stands for the weight decay regularization parameter, set at 0.005 for this CNN model. This technique minimizes the cost function and concurrently diminishes complexity, a principle referred to as structural risk minimization. [95]. In pursuit of model optimization, hyper-parameter tuning has also been performed. In this work, TensorFlow's random search is employed, executing numerous trials with random parameter combinations. Essentially, this algorithm independently selects values for each hyper-parameter using a probability distribution. Subsequently, it evaluates the cost function based on these randomly chosen hyper-parameter settings and ultimately identifies the most optimal model structure for training.

3.3 Closed-Loop Control

The objective of this study is to implement a closed-loop control strategy for the proper surface preparation of FRPC. This involves designing a feedback-based regulation mechanism to monitor resin height and adjust process parameters until the desired state is achieved without causing damage. While our experiments involved varying air pressure, SOD, and the number of passes, we have chosen to focus on controlling air pressure for the control. This decision is made because altering the SOD would also impact the blast width, and the number of passes is discrete. Therefore, establishing a connection between pressure and exposure level under controlled conditions is of significant importance to achieve our objective. Without loss of generality, we have taken data from experiments with one pass and an SOD of 3 inches, with each configuration repeated five times. Plotting these data points on a chart, as depicted in Fig. 3.5, we observe a logarithmic trend in the correlation between these two parameters:

$$P = 35.44 \ln(E) - 59.89.$$

The logarithmic trendline is accurately applied to the pressure-exposure curve, resulting in a coefficient of determination value of 0.952. This equation can also be interpreted as

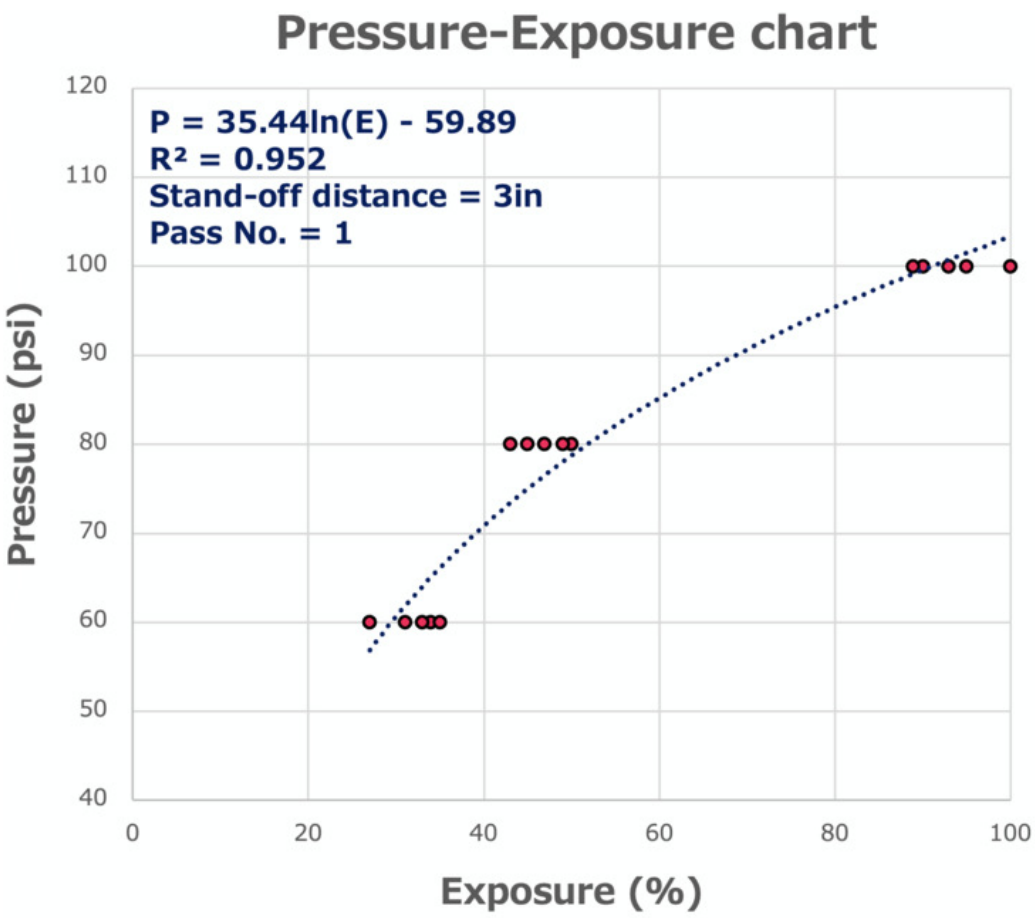

FIGURE 3.5: Exposure variations by grit blasting with three pressure values. Each data point has a stand-off distance of 3 inches and is obtained in a single pass.

the amount of resin removed with each pass of the blasting process, and the proposed closed-loop control system leverages utilizes this formulation to optimize the blasting result.

Exposure levels exceeding a threshold of 55%, traditionally regarded as over-blasted, result in wasted samples. Therefore, it is imperative to avoid reaching this state. Given the aggressive and irreversible nature of grit-blasting, our proposal is to carry out the process incrementally to ensure over-blasting is prevented. To accomplish this, we introduce a closed-loop control system, as depicted in Fig. 3.6. The process commences by capturing the surface image using a digital microscope. Subsequently, the CNN-R assesses the image to determine the surface exposure level (E_i), which is then compared to a set point representing the ideal exposure level (50%) within the control loop. This

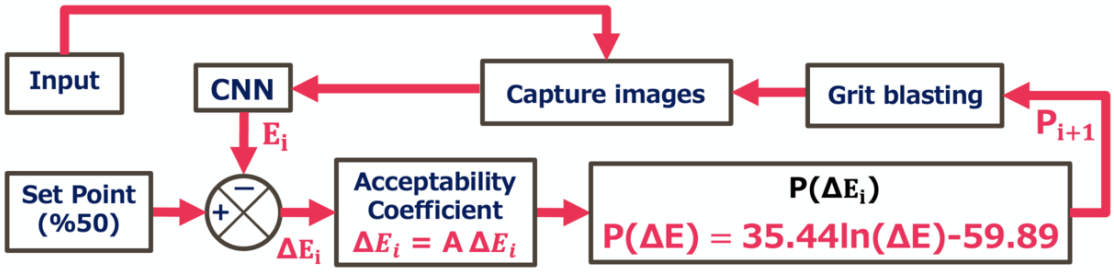

FIGURE 3.6: The proposed feedback control block diagram.

comparison yields the difference (ΔE). An acceptability coefficient (A) is introduced to safeguard against over-blasting. Taking inspiration from optimization algorithms that leverage the Golden Ratio ($\phi \approx 1.618$) to search for optimal solutions, we divide the computed removal amount by the Golden Ratio, denoted as $\Delta E/\phi$. In essence, the acceptability coefficient corresponds to the inverse of the Golden Ratio, i.e., $1/\phi \approx 0.618$, and it is multiplied by ΔE. This coefficient embodies a strategic approach aimed at achieving a balance between optimal grit-blasting pressure and risk mitigation. Subsequently, the next step utilizes the updated ΔE value to determine the pressure value (P_{i+1}) for the subsequent round of grit blasting. After the completion of each round of grit blasting, another surface image is captured, and the control loop persists until the exposure level falls within an acceptable range (within $\pm 5\%$).

4 Results & Discussions

The provided algorithm has been executed using Python on a MacBook Pro equipped with an Apple M1 Pro chip and 16GB of RAM. In this section, we will delve into the validation and verification results, along with a detailed case study.

4.1 Performance Validation

To assess the performance of our proposed network, we conducted an in-depth analysis by calculating regression errors at each epoch and presenting the results in Fig. 4.1. This comprehensive evaluation allowed us to gain valuable insights into the network's performance over the training period. As we scrutinized the convergence behavior illustrated in the figure, it became evident that the optimization process spanned a total of 70 epochs. During this period, we closely monitored the error value, observing that it reached a stable state when further changes were negligible. To gauge the network's accuracy, we opted for the Mean Absolute Error (MAE) function to quantify both training and validation errors. This selection was made deliberately, as it enables a direct interpretation of the error as a percentage deviation from the ground truth, representing the observed exposure level. This choice aligns with our objective of obtaining error metrics that closely mirror the real-world impact of deviations from the actual exposure level. It's important to emphasize that the significance of error metrics can vary depending on the specific context and application. However, for the context of our research, we established that an error within the range of $\pm 5\%$ is acceptable and does not lead to any significant alteration in the state of the grit blasting process. This tolerance threshold is practical and aligns with the objectives of our study. Upon scrutinizing the regression outcomes, we discerned the network's exceptional proficiency in forecasting the surface

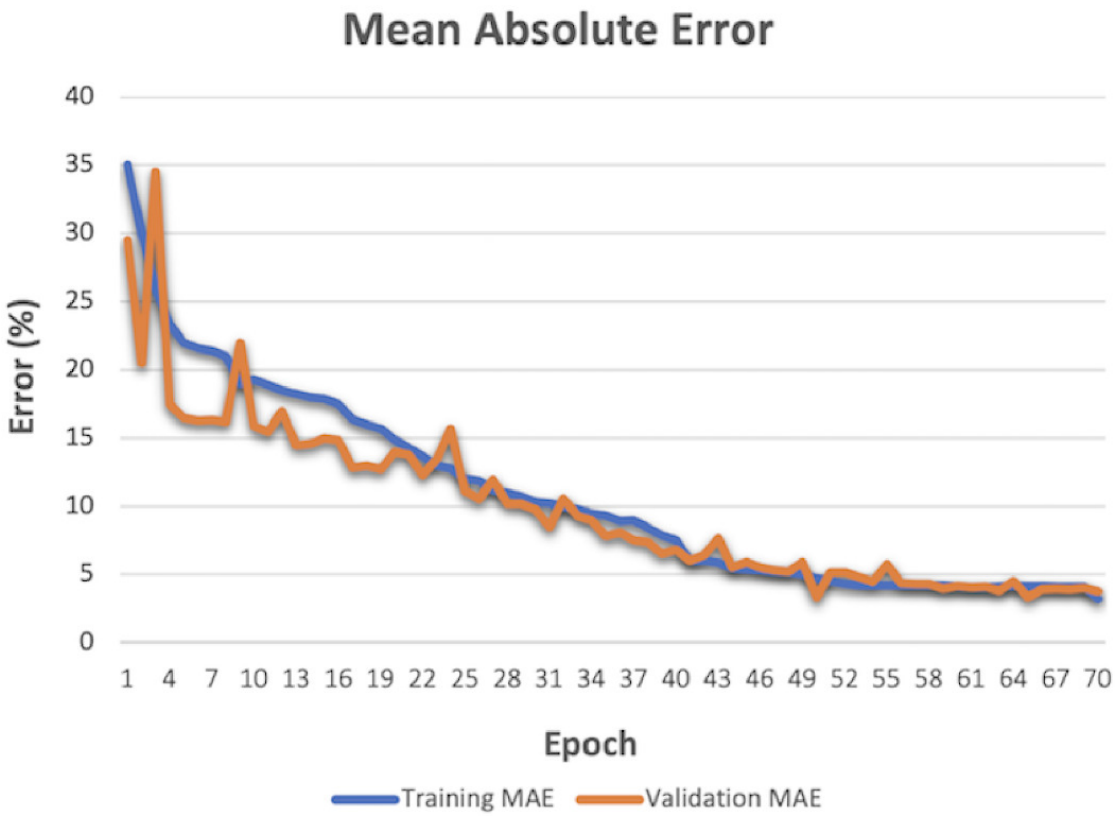

FIGURE 4.1: Mean Absolute Error (MAE) for training (Blue line) and test (Orange line) sets in 70 epochs

exposure level with remarkable precision, showcasing an impressively low error rate of approximately $\pm 3.9\%$ for both the training and validation datasets. To reiterate, our dataset comprises a total of 36,900 labeled images, with the training set consisting of 32,400 images and the validation set containing 4,500 images. This level of accuracy underscores the potential practical utility of the proposed network in real-world applications.

4.2 Feature Verification

CNNs excel in learning hierarchical features from image data, with their core components being the convolutional layers. These layers consist of multiple filters (kernels) designed to detect and extract features. In a typical CNN model, numerous layers of convolutional filters play a pivotal role in constructing informative feature maps for the

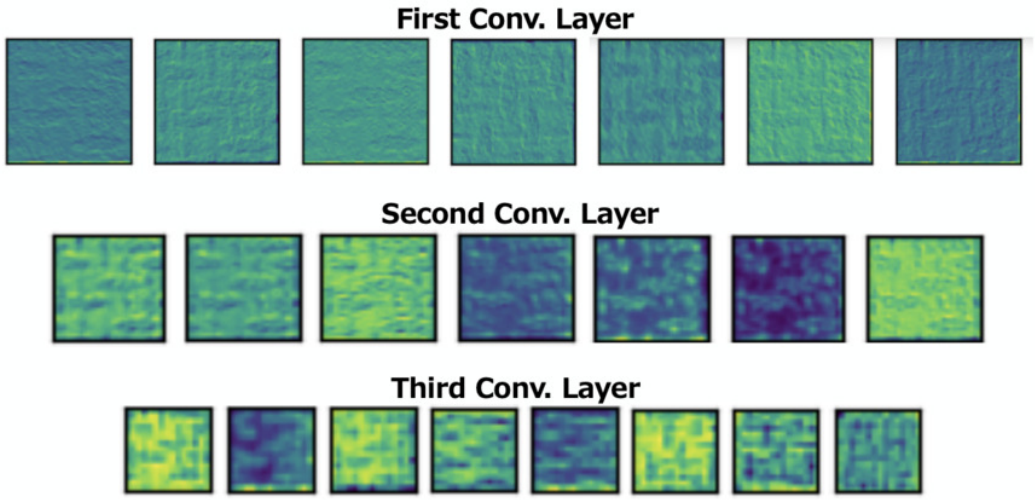

FIGURE 4.2: Visualization of activations at each convolutional layer

network's classifier. Typically, the filters in the initial layer focus on identifying broad and elementary features. As the network delves deeper, subsequent layers' filters build upon these basic features to detect increasingly intricate patterns [96]. To gain insights into and interpret the inner workings of the CNN, ensuring the meaningfulness of the learned features, we employ feature visualization techniques. These techniques generate images that maximally activate specific features within these layers. In Fig. 4.2, we present activation maps produced by the optimizer for each convolutional layer. The visualizations reveal that the first layer detects elements like blobs, edges, and variations in color between resin and metal regions, aiding in precise image segmentation. Moving to the second layer, the network begins to discern surface textures alongside its earlier knowledge of colors, lines, edges, and segments. At this stage, the CNN identifies grid-like textures on the surface, a detail not evident in the initial layer. In the third layer, the receptive field expands to unveil intricate surface patterns formed by metal mesh segments. As demonstrated by the results, this layer accentuates lower-frequency details with varying shades. These findings collectively verify the network's capability to learn and recognize dominant surface patterns at different levels of exposure to grit blasting.

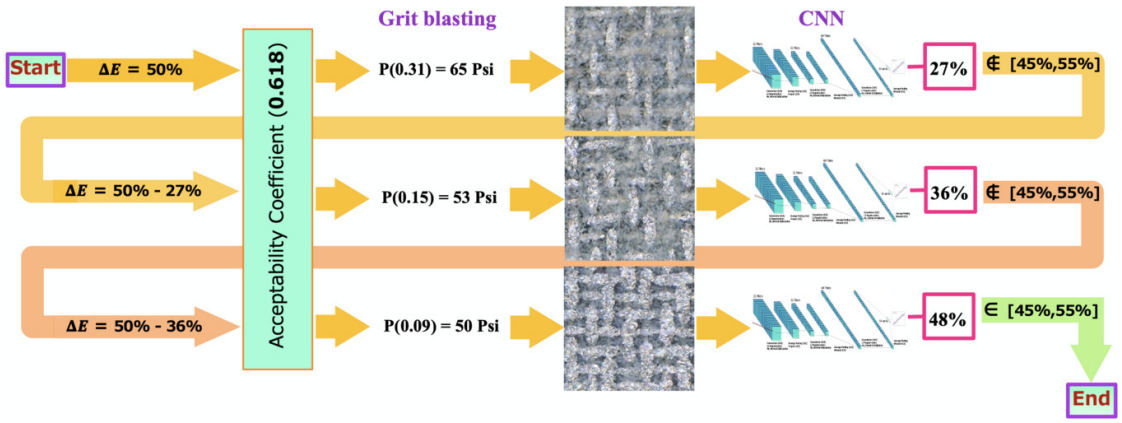

FIGURE 4.3: A case of closed-loop control procedure.

4.3 Control Case Study

We illustrate the practicality of our control system through a detailed case study, as visualized in Fig. 4.3.

The successful implementation of this approach involves a series of dynamic steps that intelligently adjust the grit blasting process to attain the desired exposure level. As depicted in the figure, the journey commences with the establishment of a target exposure of 50%. This serves as the initial goal for a surface untouched by grit blasting as it enters the control loop. However, the inherently aggressive nature of grit blasting necessitates the integration of an acceptability coefficient, set at 0.618. This adjustment reduces the target exposure to 31%, mitigating potential damage risks and preventing excessive blasting. The calculated target exposure guides the determination of the grit blasting pressure, resulting in a pressure of 0.51 MPa in this case. Grit blasting is then executed for a single pass, and the resulting surface image is fed to the CNN-R. In this scenario, CNN-R outputs an exposure of 27%, which falls below the acceptable range. Consequently, a new target exposure is computed, taking into account the acceptability coefficient, and the second round of grit blasting proceeds with the resulting pressure (0.43 MPa). This time, CNN-R outputs an exposure of 36%, which still resides outside the acceptable exposure range. Thus, the exposure difference is calculated once more, guiding the determination of a pressure of 0.41 MPa for the third round of grit

blasting. Finally, CNN-R produces an exposure estimate of 48%, aligning within the acceptable range, thereby concluding the control loop. Throughout these iterative steps, our approach demonstrates its remarkable ability to dynamically adapt the grit blasting pressure with precision and accuracy. By employing target exposure modification and leveraging CNN-R analysis, we effectively manage to achieve the desired exposure level while concurrently minimizing the risks of over-blasting or damage to the sample surface. This adaptable and responsive control mechanism has the potential to redefine grit blasting processes, ushering in an era of enhanced efficiency and meticulous quality control in surface preparation applications. This innovation holds the promise of revolutionizing surface preparation practices, optimizing outcomes, and ensuring consistency in critical industrial processes.

5 Conclusion

Coating fiber-reinforced polymer composites (FRPCs) directly with thermal spray poses a dual challenge. Not only does it risk damaging the composite surface, but it also leads to poor adhesion between the coating and the composite. To overcome these obstacles, a crucial preliminary step is required before applying the coating: attaching a metal mesh to the composite surface. This metal mesh serves two critical functions – it dissipates heat effectively and acts as an anchor, firmly securing the bond-coat to the surface. This process, involving the use of resin to affix the metal mesh to the composite, necessitates a grit-blasting step. The purpose of grit-blasting is to precisely adjust the resin level, ensuring an optimal exposure of the metal mesh. However, the conventional manual inspection of the resin level is slow and prone to inaccuracies, varying from person to person. In response to these challenges, this thesis presents a closed-loop control strategy, leveraging deep learning techniques for automated composite surface inspection. A Convolutional Neural Network for Regression (CNN-R) takes center stage in this study, monitoring the surface's exposure percentage by analyzing surface images captured with a simple digital microscope. Impressively, the proposed CNN-R is capable of determining the exposure percentage with a minimal error of approximately 4%, offering a rapid and non-destructive solution. In the course of the control process, the CNN-R's role is pivotal, ensuring precise assessment of the exposure level. To prevent material wastage, an acceptability coefficient is introduced, guaranteeing that over-blasting is avoided. This thesis represents an initial step toward the development of an online process monitoring and control system for composite manufacturing and coating. The results obtained highlight the immense promise of this research direction, showcasing

the potential for significant advancements in the realm of fast and real-time feedback-based defect detection within composite manufacturing processes. This approach holds the key to improved efficiency, enhanced product quality, and a more seamless manufacturing experience. Despite the promising outcomes, the current system remains only partially automated, necessitating human operators to load and unload parts between the grit-blasting machine and the vision inspection system. This manual involvement could potentially introduce errors in positioning and handling. To enhance the flexibility and adaptability of our approach, our future endeavors will focus on the creation of a fully automated machine. This will be accomplished by deploying high-speed microscopy cameras, strategically positioned by a robotic fixture specifically designed for precise placement, secure fixation, and subsequent removal of grit-blasted components. This fixture must possess a robust construction to enable seamless operation alongside the grit-blasting tools, ensuring accurate positioning and securing of components in front of the grit blasting gun. Additionally, it should facilitate the smooth transfer and placement of grit-blasted parts for inspection by the cameras. The integration of this advanced system holds the promise of significantly elevating both the quality and efficiency of our manufacturing process.

Bibliography

[1] Imad Shakir Abbood et al. "Properties evaluation of fiber reinforced polymers and their constituent materials used in structures–A review". In: *Materials Today: Proceedings* 43 (2021), pp. 1003–1008.

[2] Shiva Shokri et al. "A Deterministic Inspection of Surface Preparation for Metallization". In: *International Manufacturing Science and Engineering Conference*. Vol. 85802. V001T01A014. June 2022. DOI: 10.1115/MSEC2022-85334.

[3] Amrit Shankar Verma et al. "A probabilistic long-term framework for site-specific erosion analysis of wind turbine blades: A case study of 31 Dutch sites". In: *Wind Energy* (2021).

[4] Belal Alemour, Omar Badran, and Mohd Roshdi Hassan. "A review of using conductive composite materials in solving lightening strike and ice accumulation problems in aviation". In: *Journal of Aerospace Technology and Management* 11 (2019).

[5] R Gonzalez et al. "A review of thermal spray metallization of polymer-based structures". In: *Journal of Thermal Spray Technology* 25.5 (2016), pp. 897–919.

[6] Dipen Kumar Rajak et al. "Fiber-reinforced polymer composites: Manufacturing, properties, and applications". In: *Polymers* 11.10 (2019), p. 1667.

[7] Alireza Rahimi et al. "Thermal Spray Coating on Polymeric Composite for De-Icing and Anti-Icing Applications". In: *Journal of Manufacturing Science and Engineering* 143.10 (2021), p. 101008.

[8] B Tomas Åström. *Manufacturing of polymer composites*. Routledge, 2018.

[9] Hanqing Che et al. “Metallization of carbon fiber reinforced polymers for lightning strike protection”. In: *Journal of Materials Engineering and Performance* 27.10 (2018), pp. 5205–5211.

[10] Xin Zhou et al. “HVOF-Sprayed AlSi50 Alloy Coatings as a Novel Electrothermal Anti-icing/De-icing System for Polymer-based Composite Structures”. In: *Journal of Thermal Spray Technology* (2021), pp. 1–13.

[11] Adrián Lopera-Valle and André McDonald. “Flame-Sprayed Coatings as de-Icing Elements for Fiber-Reinforced Polymer Composite Structures: Modeling and Experimentation”. In: *International Journal of Heat and Mass Transfer* 97 (June 1, 2016), pp. 56–65. ISSN: 0017-9310. DOI: 10.1016/j.ijheatmasstransfer.2016.01.079.

[12] Adrián Lopera-Valle and André McDonald. “Application of flame-sprayed coatings as heating elements for polymer-based composite structures”. In: *Journal of Thermal Spray Technology* 24.7 (2015), pp. 1289–1301.

[13] Lijia Fang et al. “Cored-Wire Arc Spray Fabrication of Novel Aluminium-Copper Coatings for Anti-Corrosion/Fouling Hybrid Performances”. In: *Surface and Coatings Technology* 357 (2019), pp. 794–801.

[14] R. Kromer et al. “Laser Surface Texturing to Enhance Adhesion Bond Strength of Spray Coatings–Cold Spraying, Wire-Arc Spraying, and Atmospheric Plasma Spraying”. In: *Surface and Coatings Technology* 352 (2018), pp. 642–653.

[15] Sudarshan Devaraj et al. “Thermal Spray Deposition of Aluminum and Zinc Coatings on Thermoplastics”. In: *Surface and Coatings Technology* 399 (2020), p. 126114.

[16] V. Rat, F. Mavier, and Jean-François Coudert. “Electric Arc Fluctuations in DC Plasma Spray Torch”. In: *Plasma Chemistry and Plasma Processing* 37 (2017), pp. 549–580.

[17] Mitchell R. Dorfman. “Chapter 22 - Thermal Spray Coatings”. In: *Handbook of Environmental Degradation of Materials (Third Edition)*. Ed. by Myer Kutz. William Andrew Publishing, Jan. 1, 2018, pp. 469–488. ISBN: 978-0-323-52472-8. DOI: 10.1016/B978-0-323-52472-8.00023-X.

[18] Christophe Chazelas, J. P. Trelles, and A. Vardelle. "The Main Issues to Address in Modeling Plasma Spray Torch Operation". In: *Journal of Thermal Spray Technology* 26 (2017), pp. 3–11.

[19] Sina Mirzai Tavana et al. "Erosion Resistance Enhancement of Polymeric Composites with Air Plasma Sprayed Coatings". In: *Surface and Coatings Technology* 455 (Feb. 25, 2023), p. 129211. ISSN: 0257-8972. DOI: 10.1016/j.surfcoat.2022.129211.

[20] Lukas Kinner, Emil JW List-Kratochvil, and Theodoros Dimopoulos. "Gentle Plasma Process for Embedded Silver-Nanowire Flexible Transparent Electrodes on Temperature-Sensitive Polymer Substrates". In: *Nanotechnology* 31.36 (2020), p. 365303.

[21] Alireza Rahimi et al. "Thermal Spray Coating on Polymeric Composite for De-Icing and Anti-Icing Applications". In: *Journal of Manufacturing Science and Engineering* 143.101008 (Apr. 30, 2021). ISSN: 1087-1357. DOI: 10.1115/1.4050650.

[22] Jiayu Sun et al. "Adhesion mechanism of temperature effects on Sn coating on the carbon fiber reinforced polymer substrate by cold spray". In: *arXiv preprint arXiv:2010.10988* (2020).

[23] Hanqing Che et al. "Metallization of various polymers by cold spray". In: *Journal of Thermal Spray Technology* 27.1 (2018), pp. 169–178.

[24] Jiayu Sun et al. "Thermal Effects in Sn Coating on a Carbon Fiber Reinforced Plastic by Cold Spraying". In: *Journal of Thermal Spray Technology* 30.5 (2021), pp. 1254–1261.

[25] Hanqing Che et al. "Metallization of Polymers by Cold Spraying with Low Melting Point Powders". In: *Surface and Coatings Technology* 418 (2021), p. 127229.

[26] Amos Adeniyi et al. "Thermoplastic-thermoset nanostructured polymer blends". In: *Design and Applications of Nanostructured Polymer Blends and Nanocomposite Systems*. Elsevier, 2016, pp. 15–38.

[27] Anup K Ghosh and Mayank Dwivedi. "Processability in Open Mould Processing of Polymeric Composites". In: *Processability of Polymeric Composites*. Springer, 2020, pp. 179–203.

[28] Panteha Fallah et al. "Development of hybrid metallic coatings on carbon fiber-reinforced polymers (CFRPs) by cold spray deposition of copper-assisted copper electroplating process". In: *Surface and Coatings Technology* 400 (2020), p. 126231.

[29] Vincent Bortolussi et al. "Electrical conductivity of metal–polymer cold spray composite coatings onto carbon fiber-reinforced polymer". In: *Journal of Thermal Spray Technology* 29.4 (2020), pp. 642–656.

[30] Rafael Gonzalez and Richard Woods. *Digital image processing*. Pearson, 2017.

[31] Mark Nixon and Alberto Aguado. *Feature extraction and image processing for computer vision*. Academic press, 2019.

[32] Henry O Velesaca et al. "Computer vision based food grain classification: A comprehensive survey". In: *Computers and Electronics in Agriculture* 187 (2021), p. 106287.

[33] Tianjiao Wang et al. "In-situ droplet inspection and closed-loop control system using machine learning for liquid metal jet printing". In: *Journal of Manufacturing Systems* 47 (2018), pp. 83–92. ISSN: 0278-6125. DOI: 10.1016/j.jmsy.2018.04.003.

[34] Swarit Anand Singh and K. A. Desai. "Automated Surface Defect Detection Framework Using Machine Vision and Convolutional Neural Networks". In: *Journal of Intelligent Manufacturing* 34.4 (2023), pp. 1995–2011. ISSN: 1572-8145. DOI: 10.1007/s10845-021-01878-w.

[35] Mustafa Ozuysal et al. "Fast Keypoint Recognition Using Random Ferns". In: *IEEE transactions on pattern analysis and machine intelligence* 32.3 (Mar. 2010), pp. 448–461. ISSN: 1939-3539. DOI: 10.1109/TPAMI.2009.23. pmid: 20075471.

[36] Matthew Brown and David G. Lowe. "Automatic Panoramic Image Stitching Using Invariant Features". In: *International Journal of Computer Vision* 74.1 (Aug. 1, 2007), pp. 59–73. ISSN: 1573-1405. DOI: 10.1007/s11263-006-0002-3.

[37] Somya Jain. "Edge Detection Using Fuzzy Gradient Information". Pat. 20200027214. Adobe Inc. (San Jose, CA, US). Jan. 23, 2020.

[38] G T Shrivakshan. "A Comparison of Various Edge Detection Techniques Used in Image Processing". In: 9.5 (2012).

[39] Yun Liu et al. "Richer Convolutional Features for Edge Detection". In: *IEEE Transactions on Pattern Analysis and Machine Intelligence* 41.8 (Aug. 1, 2019), pp. 1939–1946. ISSN: 0162-8828, 2160-9292, 1939-3539. DOI: 10.1109/TPAMI.2018.2878849.

[40] Longfei Zhou, Lin Zhang, and Nicholas Konz. "Computer Vision Techniques in Manufacturing". In: *IEEE Transactions on Systems, Man, and Cybernetics: Systems* 53.1 (Jan. 2023), pp. 105–117. ISSN: 2168-2232. DOI: 10.1109/TSMC.2022.3166397.

[41] Tony Lindeberg. "Scale Invariant Feature Transform". In: *Scholarpedia* 7.5 (May 22, 2012), p. 10491. ISSN: 1941-6016. DOI: 10.4249/scholarpedia.10491.

[42] Yong Ma et al. "Robust Image Feature Matching via Progressive Sparse Spatial Consensus". In: *IEEE Access* 5 (2017), pp. 24568–24579. DOI: 10.1109/ACCESS.2017.2768078.

[43] Yi Sun et al. *DeepID3: Face Recognition with Very Deep Neural Networks*. Feb. 3, 2015. DOI: 10.48550/arXiv.1502.00873. arXiv: 1502.00873 [cs].

[44] Lei Wu, Steven C H Hoi, and Nenghai Yu. "Semantics-Preserving Bag-of-Words Models and Applications". In: *IEEE Transactions on Image Processing* 19.7 (July 2010), pp. 1908–1920. ISSN: 1057-7149, 1941-0042. DOI: 10.1109/TIP.2010.2045169.

[45] Kaiming He et al. "Deep Residual Learning for Image Recognition". In: *2016 IEEE Conference on Computer Vision and Pattern Recognition (CVPR)*. June 2016, pp. 770–778. DOI: 10.1109/CVPR.2016.90.

[46] Li Chen et al. "Survey of Pedestrian Action Recognition Techniques for Autonomous Driving". In: *Tsinghua Science and Technology* 25.4 (Aug. 2020), pp. 458–470. ISSN: 1007-0214.

[47] Po-Chun Hsu et al. "A Dual-Mode Textile for Human Body Radiative Heating and Cooling". In: *Science Advances* 3.11 (Nov. 2017), e1700895. ISSN: 2375-2548. DOI: 10.1126/sciadv.1700895. pmid: 29296678.

[48] Daniel Cremers, Mikael Rousson, and Rachid Deriche. "A Review of Statistical Approaches to Level Set Segmentation: Integrating Color, Texture, Motion and Shape". In: *International Journal of Computer Vision* 72.2 (Apr. 1, 2007), pp. 195–215. ISSN: 1573-1405.

[49] D. Comaniciu and P. Meer. "Mean Shift: A Robust Approach toward Feature Space Analysis". In: *IEEE Transactions on Pattern Analysis and Machine Intelligence* 24.5 (May 2002), pp. 603–619. ISSN: 1939-3539. DOI: 10.1109/34.1000236.

[50] Yuri Boykov and Gareth Funka-Lea. "Graph Cuts and Efficient ND Image Segmentation". In: *International Journal of Computer Vision - IJCV* 70 (Nov. 1, 2006), pp. 109–131. DOI: 10.1007/s11263-006-7934-5.

[51] Jieneng Chen et al. *TransUNet: Transformers Make Strong Encoders for Medical Image Segmentation*. 2021. arXiv: 2102.04306 [cs.CV].

[52] J. Aloimonos. "Shape from Texture". In: *Biological Cybernetics* 58.5 (1988), pp. 345–360. ISSN: 0340-1200. DOI: 10.1007/BF00363944. pmid: 3382705.

[53] S.K. Nayar and Y. Nakagawa. "Shape from Focus". In: *IEEE Transactions on Pattern Analysis and Machine Intelligence* 16.8 (Aug. 1994), pp. 824–831. ISSN: 1939-3539. DOI: 10.1109/34.308479.

[54] Berthold Horn. "Shape from Shading: A Method for Obtaining the Shape of a Smooth Opaque Object from One View". In: (Oct. 20, 2004).

[55] Yutong Fu and Xuefeng Yao. "A Review on Manufacturing Defects and Their Detection of Fiber Reinforced Resin Matrix Composites". In: *Composites Part C: Open Access* 8 (2022), p. 100276.

[56] Alessio Trolli et al. "Characterization of porosity and defects on composite materials using X-ray computed tomography and image processing". In: *2021 IEEE*

8th International Workshop on Metrology for AeroSpace (MetroAeroSpace). IEEE. 2021, pp. 479–484.

[57] H. Elbehiery, Alaa A. Hefnawy, and M. Tarek Elewa. "Surface Defects Detection for Ceramic Tiles Using Image Processing and Morphological Techniques". In: *WEC*. 2005.

[58] Uroš Hudomalj et al. "Analysis and Comparison of Two Different Sensing Techniques for In Situ Coating Thickness Measurements". In: *Journal of Thermal Spray Technology* 32.2-3 (2023), pp. 673–680.

[59] Uroš Hudomalj et al. "A Novel Approach to In Situ Coating Thickness Measurements in Thermal Spraying". In: *ITSC 2023*. ASM International, 2023, pp. 142–147.

[60] Kung-Jeng Wang, Hao Fan-Jiang, and Ya-Xuan Lee. "A Multiple-Stage Defect Detection Model by Convolutional Neural Network". In: *Computers & Industrial Engineering* 168 (2022). ISSN: 0360-8352. DOI: 10.1016/j.cie.2022.108096.

[61] Vikas Sharma, Joy Prakash Misra, and Sandeep Singhal. "Surface Roughness Modeling Using Machine Learning Approaches for Wire Electro-Spark Machining of Titanium Alloy". In: *International Journal of Structural Integrity* 13.6 (2022), pp. 999–1012. ISSN: 1757-9864. DOI: 10.1108/IJSI-08-2022-0108.

[62] Moncef Soualhi, Khanh T. P. Nguyen, and Kamal Medjaher. "Pattern Recognition Method of Fault Diagnostics Based on a New Health Indicator for Smart Manufacturing". In: *Mechanical Systems and Signal Processing* 142 (Aug. 1, 2020), p. 106680. ISSN: 0888-3270. DOI: 10.1016/j.ymssp.2020.106680.

[63] Aravinda S. Rao et al. "Real-Time Monitoring of Construction Sites: Sensors, Methods, and Applications". In: *Automation in Construction* 136 (2022), p. 104099. ISSN: 0926-5805. DOI: 10.1016/j.autcon.2021.104099.

[64] Pooria Sedigh Rahimabadi. *Surface Preparation of Polymer Composites Embedded Metal Mesh for Coating Using Optimized Grit-Blasting Process*. 2022.

[65] Mutasem K Alsmadi. "Content-based image retrieval using color, shape and texture descriptors and features". In: *Arabian Journal for Science and Engineering* 45.4 (2020), pp. 3317–3330.

[66] Nicolas Duboust et al. "Towards intelligent CFRP composite machining: Surface analysis methods and statistical data analysis of machined fibre laminate surfaces". In: *Proceedings of the Institution of Mechanical Engineers, Part B: Journal of Engineering Manufacture* 235.10 (2021), pp. 1602–1617.

[67] Thomas Lacombe, Hugues Favreliere, and Maurice Pillet. "Modal Features for Image Texture Classification". In: *Pattern Recognition Letters* 135 (2020), pp. 249–255. ISSN: 0167-8655. DOI: 10.1016/j.patrec.2020.04.036.

[68] Rik Das. *Content-Based Image Classification: Efficient Machine Learning Using Robust Feature Extraction Techniques*. Boca Raton, FL: CRC Press, 2020.

[69] Vahid Nasir and Farrokh Sassani. "A Review on Deep Learning in Machining and Tool Monitoring: Methods, Opportunities, and Challenges". In: *The International Journal of Advanced Manufacturing Technology* 115 (2021). DOI: 10.1007/s00170-021-07325-7.

[70] Alicia Passah et al. "SAR Image Classification: A Comprehensive Study and Analysis". In: *IEEE Access* 10 (2022). DOI: 10.1109/ACCESS.2022.3151089.

[71] D. R. Sarvamangala and Raghavendra V. Kulkarni. "Convolutional Neural Networks in Medical Image Understanding: A Survey". In: *Evolutionary intelligence* 15.1 (2022), pp. 1–22.

[72] Pengxiang Shi et al. "Dual Convolutional Neural Network for Lung Nodule Classification". In: *2021 International Joint Conference on Neural Networks (IJCNN)*. IEEE, 2021, pp. 1–7.

[73] Jianjun Yan et al. "Tongue Image Texture Classification Based on Image Inpainting and Convolutional Neural Network." In: *Computational and mathematical methods in medicine* 2022 (2022), p. 6066640. ISSN: 1748-670X. DOI: 10.1155/2022/6066640.

[74] Arohan Ajit, Koustav Acharya, and Abhishek Samanta. "A Review of Convolutional Neural Networks". In: *2020 International Conference on Emerging Trends in Information Technology and Engineering (Ic-ETITE)*. IEEE, 2020, pp. 1–5.

[75] D. H. Hubel and T. N. Wiesel. "Receptive Fields, Binocular Interaction and Functional Architecture in the Cat's Visual Cortex". In: *The Journal of Physiology* 160.1 (1962), pp. 106–154. ISSN: 1469-7793. DOI: 10.1113/jphysiol.1962.sp006837.

[76] Ivana Strumberger et al. "Convolutional Neural Network Architecture Design by the Tree Growth Algorithm Framework". In: *2019 International Joint Conference on Neural Networks (IJCNN)*. IEEE, 2019, pp. 1–8.

[77] Milan Tripathi. "Analysis of Convolutional Neural Network Based Image Classification Techniques". In: *Journal of Innovative Image Processing (JIIP)* 3.02 (2021), pp. 100–117.

[78] Jiang Wang et al. "CNN-RNN: A Unified Framework for Multi-Label Image Classification". In: Proceedings of the IEEE Conference on Computer Vision and Pattern Recognition. 2016, pp. 2285–2294.

[79] Sumeet S. Shah, John W. Sheppard, and United Kingdom 2020 July 19 2020 July 2020 International Joint Conference on Neural Networks (IJCNN) Glasgow. "Evaluating Explanations of Convolutional Neural Network Image Classifications". In: *2020 International Joint Conference on Neural Networks (IJCNN)*. IEEE, 2020, pp. 1–8.

[80] "Closed-Loop Control". In: *Flow Control Techniques and Applications*. Ed. by Jinjun Wang and Lihao Feng. Cambridge Aerospace Series. Cambridge: Cambridge University Press, 2018, pp. 266–277. DOI: 10.1017/9781316676448.012.

[81] Behnood Gholami et al. "Closed-Loop Control for Fluid Resuscitation: Recent Advances and Future Challenges". In: *Frontiers in Veterinary Science* 8 (2021). ISSN: 2297-1769.

[82] Xing Fang and Wen-Hua Chen. *Model Predictive Control with Preview: Recursive Feasibility and Stability*. 2022. DOI: 10.48550/arXiv.2202.12585. arXiv: 2202.12585 [cs, eess].

[83] Ziyad Smoqi et al. "Closed-Loop Control of Meltpool Temperature in Directed Energy Deposition". In: *Materials & Design* 215 (2022), p. 110508.

[84] M. Priyadharshini et al. "Fiber Reinforced Composite Manufacturing with the Aid of Artificial Intelligence–A State-of-the-Art Review". In: *Archives of Computational Methods in Engineering* 29.7 (2022), pp. 5511–5524.

[85] Itzel De Jesus Gonzalez Ojeda, Olivier Patrouix, and Yannick Aoustin. "Pressure Based Approach for Automated Fiber Placement (AFP) with Sensor Based Feedback Loop and Flexible Component in the Effector". In: *IFAC-PapersOnLine* 50.1 (2017), pp. 794–799. ISSN: 24058963. DOI: 10.1016/j.ifacol.2017.08.511.

[86] Julian Seuffert et al. "Experimental and Numerical Investigations of Pressure-Controlled Resin Transfer Molding (PC-RTM)". In: *Advanced Manufacturing: Polymer & Composites Science* 6.3 (Aug. 7, 2020), pp. 154–163. ISSN: 2055-0340. DOI: 10.1080/20550340.2020.1805689.

[87] Georg Mauer and Christian Moreau. "Process Diagnostics and Control in Thermal Spray". In: *Journal of thermal spray technology* 31.4 (2022), pp. 818–828.

[88] Lu Lu et al. "In-Situ Process Evaluation for Continuous Fiber Composite Additive Manufacturing Using Multisensing and Correlation Analysis". In: *Additive Manufacturing* (2023), p. 103721.

[89] Balachandar Guduri. "Modified Robust Adaptive Process Control with Improved Transient Performance and Its Application to Atmospheric Plasma Spray Process". In: (2023).

[90] Lu Lu et al. "Deep Learning-Assisted Real-Time Defect Detection and Closed-Loop Adjustment for Additive Manufacturing of Continuous Fiber-Reinforced Polymer Composites". In: *Robotics and Computer-Integrated Manufacturing* 79 (2023), p. 102431.

[91] Chenang Liu et al. "Image Analysis-Based Closed Loop Quality Control for Additive Manufacturing with Fused Filament Fabrication". In: *Journal of Manufacturing Systems* 51 (2019), pp. 75–86.

[92] Ronan McCann et al. “In-Situ Sensing, Process Monitoring and Machine Control in Laser Powder Bed Fusion: A Review”. In: *Additive Manufacturing* 45 (2021), p. 102058. ISSN: 22148604. DOI: 10.1016/j.addma.2021.102058.

[93] Wenling Shang et al. “Understanding and Improving Convolutional Neural Networks via Concatenated Rectified Linear Units”. In: *Proceedings of The 33rd International Conference on Machine Learning*. Ed. by Maria Florina Balcan and Kilian Q. Weinberger. Vol. 48. Proceedings of Machine Learning Research. New York, New York, USA: PMLR, 2016, pp. 2217–2225.

[94] Yifeng Wang et al. “PCA Based Kernel Initialization for Convolutional Neural Networks”. In: *Data Mining and Big Data: 5th International Conference, DMBD 2020, Belgrade, Serbia, July 14–20, 2020, Proceedings 5*. Springer, 2020, pp. 71–82.

[95] QiuChen Feng, Dongliang Peng, and Yu Gu. “Research of Regularization Techniques for SAR Target Recognition Using Deep CNN Models”. In: *Tenth International Conference on Graphics and Image Processing (ICGIP 2018)*. Vol. 11069. SPIE, 2019, pp. 1066–1073. DOI: 10.1117/12.2524147.

[96] Anh Nguyen, Jason Yosinski, and Jeff Clune. “Multifaceted feature visualization: Uncovering the different types of features learned by each neuron in deep neural networks”. In: *arXiv:1602.03616* (2016).